IASJ
المجلات الاكاديمية العراقية

Tikrit Journal of Pure Science
ISSN: 1813 – 1662 (Print) --- E-ISSN: 2415 – 1726 (Online)

Journal Homepage: http://tjps.tu.edu.iq/index.php/j

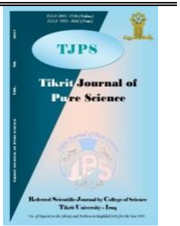

Differentiation of Multi-lithotypes Olistostromal Occurrences Associated with Iron Enrichment and Mineralization Within the Ophiolites of Choman Area, NE Iraq

Barzan K. Azo[1] , Kamal Kolo[2] , Mohammad Pirouei [2]
[1]*Department of Petroleum Geoscience, Faculty of Science, Soran University, Soran, KRG, Iraq*
[2]*Scientific Research Center (SRC), Soran University, Soran, KRG, Iraq*

https://doi.org/10.25130/tjps.v28i2.1335

ARTICLE INFO.

Article history:
-Received: 9 / 8 / 2022
-Accepted: 15 / 9 / 2022
-Available online: 26 / 4 / 2023

Keywords: Olistostromes; Mélange; Rayat; Lithoclast; FCO.

Corresponding Author:
Name: Barzan K. Azo
E-mail: bka040h@petg.soran.edu.iq
kamal.kolo@soran.edu.iq
mohammad.askandar@soran.edu.iq
Tel:

ABSTRACT

The discovery of multi-lithotypes olistostromes deposits associated with potentially economically viable iron ore mineralizations in the Rayat region of NE Iraq are described in this study. The depositional and differentiation-classification characteristics of multi-lithotypes of olistostromes with distinct depositional and characteristics are reported here through detailed petrographic, mineralogical, and geochemical data, allowing for mineralization mechanisms assessment and associated hydrothermal and alteration processes. Ferruginous conglomerate lithotypes occur below the sandstone olistostromes lithotypes section of the investigated series. Through the ferruginous conglomerate olistostromes (FCO) lithotypes, there is a layer of potentially iron ore containing iron oxide (up to %42.55) and quartz with some minor spinel content. Below FCO, there are the horizons of FOpO and FSO, which are also rich in hematite quartz and calcite with some minor spinel content. A 2m thick transition zone (TZ) separates the poorly mineralized ophiocarbonatic olistostrome (OpCO) from FCO. The multi-lithotypes of olistostrome from bottom to top are serpentinite olistostrome (SO), ophiocarbonatic olistostrome (OpCO), ferruginous serpentinite olistostrome (FSO), ferruginous ophiocarbonatic olistostrome (FOpCO), ferruginous conglomerate olistostrome (FCO), and sandstone olistostrome (SstO). In addition to Fe, the other potential economic important elements include nickel (507 to 5816 mg/kg) and cobalt (47.2 to 328.3 mg/kg). The findings indicate that the Rayat olistostromes, such as SO, FSO, OpCO, FOpCO, FCO, and SstO, and the transition zone (TZ) are originated from a mixture of early hydrothermal alteration of serpentinites. The finding of olistostromes in the Rayat exposes NE Iraq as a potential mineral-rich sector.

1. Introduction

Flores [82] used the term "olistostrome," which is derived from the Greek words "olistomai" (to slide) and "strome" (accumulation), to indicate sediment accumulation induced by gravity sliding in a process defined as submarine sliding of Mass Transport Complex (M.T.C.). He additionally mentioned that olistostromes should be sufficiently continuous to be mappable. Generally, olistostromes from the lithological point of view are heterogeneous, more or less admixed, lack real bedding, and are formed by the rapid accumulation of rocks, fragments and blocks [1, 2]. Additionally, they contain fine to coarse sediments and lithoclasts in the form of a semifluid mass that can show vertical and/or horizontal gradation. The lithoclasts (also called olistoliths) embedded in these accumulations are derived from former deposits [3]. The accumulated end product of those unconsolidated sediments has been defined as olistostromes [4].

Many authors [1, 2, 5-7] have discussed the conceptual definition of olistostromes and mélanges and how they are differentiated. Both rock bodies are composed of blocks in a shattered finer-grained matrix and are distinguished by a lack of stratal continuity throughout their entire lengths of exposure. A common view adopted here is that olistostromes are sedimentary deposits produced by gravity mass flows, defined as Mass Transport Complexes (M.T.C.s) [2, 9, 10]. In contrast, mélanges are sedimentary deposits formed by sedimentary processes, faulting, and tectonic shearing [11]. The existence of sheer fabric in the matrix, in particular, is widely regarded as a distinguishing trait of a mélange.

Other tectonic habitats, such as passive continental margins, have been postulated as potential mélanges and olistostromes development sites. Subduction zones are the most commonly seen tectonic environments for the production of these fractured and mixed rock masses [7]. All across the course of passive margin development, rifting tectonics and rifting-related geological events often result in the production of distinct forms of olistostromes. These olistostromes arise at the margins of thinning carbonate platforms and continental margins, at ocean-continent transition zones (OCT), and about oceanic core clusters.

Mineralization in N and NE Iraq has been documented to be of magmatic, hydrothermal, metamorphic, and sedimentary origin [13-15]. The principal minerals in N and NE Iraq are oxides, such as Cr- and Ni-rich deposits in Mawat Penjween and Rawanduz [16-18]. While iron ore deposits are often tiny and structurally classified as endogenic contact-metasomatic substitution, magmatic, and sedimentary ironstone [15, 19].

The Triassic-Jurassic Zn-Pb mineralization phase has been also reported and reliably dated in the Shalair District as the Marabasta deposit [20]. The olistostromes of the Rayat area are composed of different lithotypes. Some of those lithotypes are ferruginous, rich in iron, and some other elements, such as Ni and Co. In this research, the geological context, petrographical and geochemical properties of the olistostromes occurrences in the Rayat area, NE Iraqi Kurdistan are discussed, and their economic potential is highlighted.

2. Geological Setting

The study area is located in the northeastern corner of Iraq near the Iraqi-Iranian border (Fig. 1a). Geotectonically, the area is part of the Iraqi Zagros Suture Zone (IZSZ), which is the most deformed zone of the ongoing collision between the Arabian Plate and Anatolian microcontinent to the north, and Arabian and Iranian Plates towards northeastern Iraq [21]. IZSZ comprises three tectonic subzones (Fig. 1b), namely, Shalair, Penjween-Walash, and Qulqula-Khwakurk [13, 22]. The study area is geologically delimited by the undifferentiated Paleocene-Upper Eocene lithostratigraphic units of the Walash Group, within the Penjween-Walash subzone (Fig.1). The Walash Group rocks are covered in places by Quaternary sediments, mostly in the form of talus and terrace deposits [23]. The primary rock types of the Walash Group that outcrop in the broader Rayat area are sedimentary, volcano-sedimentary, and intrusive rocks, with the latter being mostly serpentinized peridotites [23]. A significant aspect of the geological framework of the area is that the encountered lithologies, apart from the newly discovered olistostromes, represent the ophiolitic mélange of the ophiolite nappe. Hence, the various groups are generally in a chaotic mixture with no clear boundaries (Fig. 2).

Generally, in addition to the Quaternary sediments and intrusive rocks, the sedimentary rocks outcropping in the area include red and light greenish calcareous argillites. In addition, subsidiary brown ferruginous conglomerates, red siliceous-jasper rocks, and reddish-grey sandstone are occurring. The other units have a volcano-sedimentary group, consisting of basalts, conglomerates, and tuffite with Eocene age [23]. Intrusive igneous rocks that occur as sheets and sills of altered ultramafic rocks are massive, granular, and aphanitic serpentinites derived from the metasomatic alteration of ultramafic rocks, with chromatic lenses, occasionally hosted within the sheared varieties of serpentinites. The later hydrothermal alteration of the serpentinites causes the formation of listvenite and fuchsite in the area [24, 25]. Based on stratigraphy, Eocene age was assigned to the Walash Group rocks [26], but according to the radiometric dating by 40Ar–39Ar of its basaltic rocks, an age range of 24–43 Ma (Eocene–Oligocene) was demonstrated [27].

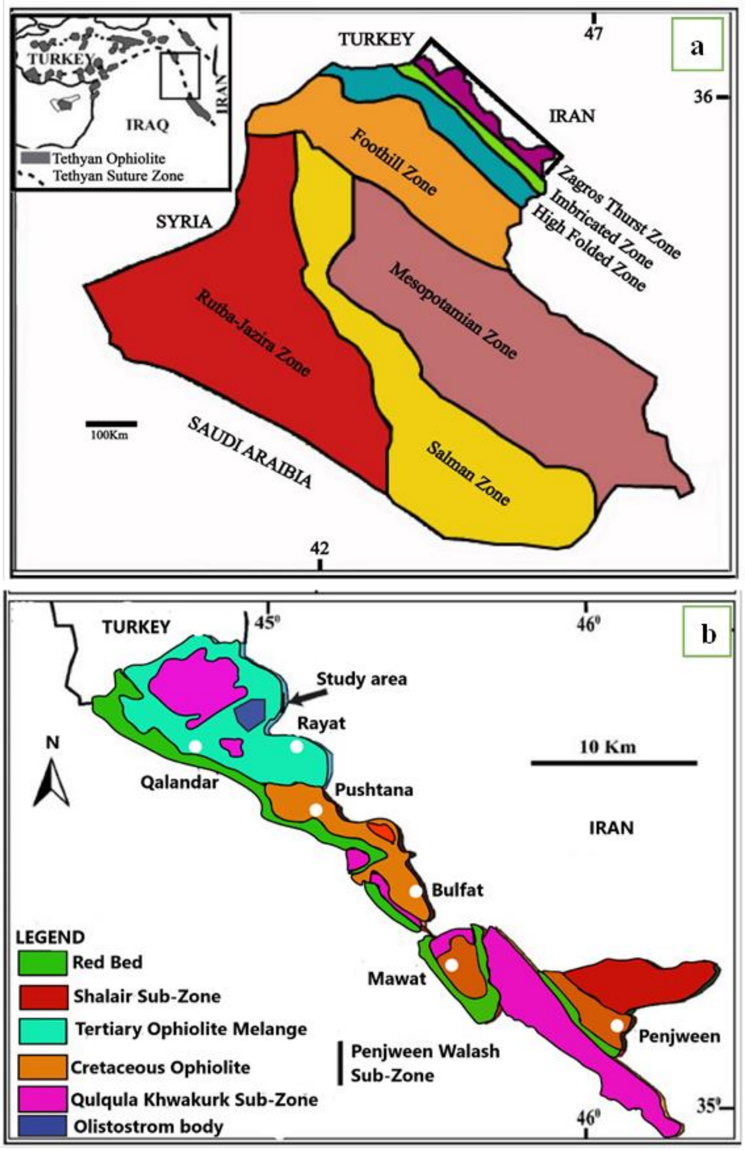

Fig. 1: a) Updated tectonic map showing tectonic zones between Iraq and Iran in the Zagros Mountains (based on [28] and modified by [29]), (b) a comprehensive geological map of the greater Rayat area in northeast Iraq (based on [28] and modified by [29])

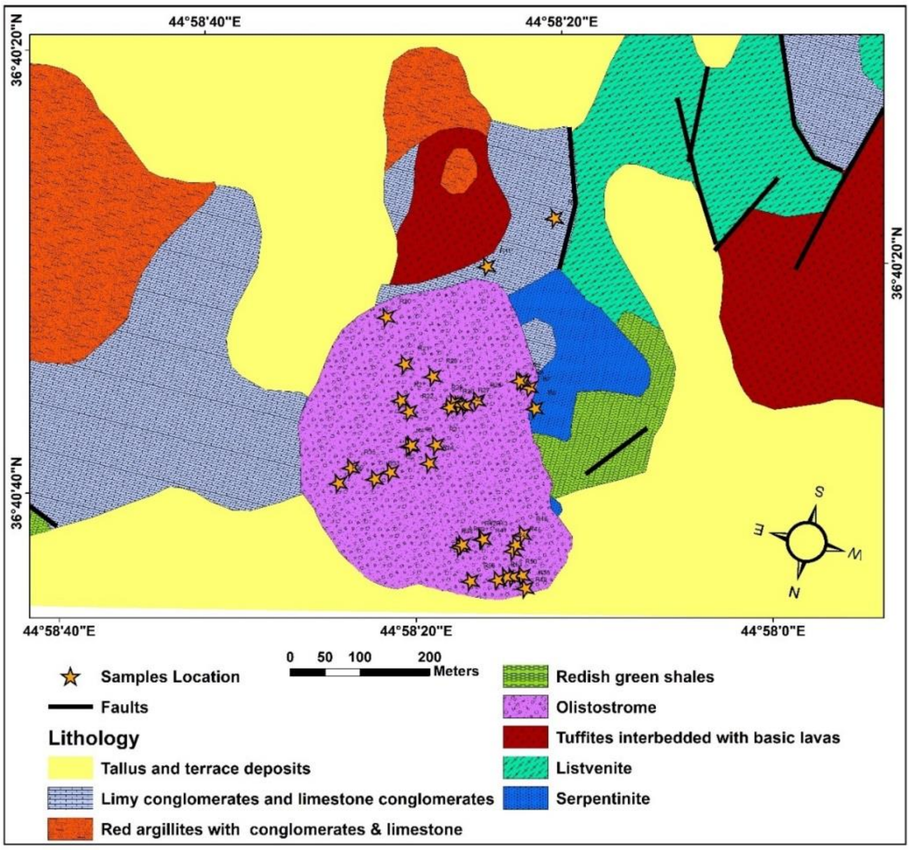

Fig. 2: Updated geological map of the Rayat area based on the current study showing new rock types of olistostromes and listvenites adapted from [23] and [25]

3. Materials and Methods

3.1 Sampling

Several reconnaissance and exploration fieldwork trips were carried out in the area to record the field observations and sampling. During the field trips, the outcrops of the olistostromes were identified, mapped, and sampled. Thirty-seven samples were collected from the outcrops and the nearby rocks (Fig. 2) for petrographic, mineralogical, and geochemical studies. All the samples were described, labeled, and coordinated with GPS in the field.

3.2 Petrographical Studies

Thirty-four (34) doubly polished thin sections were prepared from the numerous olistostrome lithotypes and the surrounding rocks. They were studied using a LEICA DM4500P polarized light microscope. The petrographic examination of the thin-polished sections involved the identification of mineral assemblages, as well as of bio clasts and fossils, followed by the characterization of textures, diagenetic features, and the selection of representative spots of interest for the detailed imaging, mapping, and elemental study using scanning electron microscopy with energy-dispersive X-ray spectroscopy (SEM-EDS). The SEM-EDS examination was carried out on gold-coated thin polished sections and on rock slabs with a FEI 480 SEM coupled with a BRUKER-QUANTAX energy dispersive X-ray spectroscopy at accelerating voltage of 15 – 25 kV, beam current of 20 nA, beam size, 1-2 µm, and count time of 20 s at the facilities of Scientific Research Center of Soran University.

3.3 Mineralogical Determinations

X-ray diffraction (XRD) examinations were performed using a PANalytical X'Pert PRO MPD Alpha powder diffractometer in Bragg Brentano $\theta/2\theta$ geometry of 240 mm radius, Cu-filtered Kα radiation ($\lambda = 1.5418$ Å) at 45 kV and 40 mA at the facilities of the Scientific Research Center of Soran University, Iraq. The scanning parameters were as follows: $2\theta = 6–88^{\circ}$, with a step size of 0.017° and step time of 50 s, using an X'Celerator detector (active length = 2.122°). A qualitative evaluation and semi-quantification of the mineral phases were performed using High-Score Plus software® at the Scientific Research Center of Soran University.

3.4 Geochemical Analyses

Whole rock geochemical analysis for the determination of the major and minor elements was performed on powdered samples by using inductivity coupled plasma atomic emission spectroscopy (ICP-OES) for major elements and inductivity coupled plasma mass spectrometry (ICP-MS) for minor and trace elements at Zarazma laboratory in Iran by applying lithium borate fusion of the sample before acid dissolution. Loss on ignition (LOI) values were determined by the combustion of 1g at 950° C for two hours using a Selecta® muffle furnace.

4. Results

4.1 Field Observations

The fieldwork surveyed partially outcropping olistostrome bodies located in the south of the Rayat village (Fig. 2). The olistostrome outcrops lithologies can be categorized into distinct lithotypes that are bounded by other rock types of sedimentary and igneous rocks, such as limestones, sandstone and serpentinized peridotites (Fig.3). The generalized cross-section of the olistostrome bodies from bottom to top (Fig. 4) mapped in the field showed: serpentinite olistostrome (SO), ophiocarbonatic olistostrome (OpCO), ferruginous serpentinite olistostrome (FSO), ferruginous ophiocarbonatic olistostrome (FOpCO), transition zone (T.Z.), ferruginous conglomerate olistostromes (FCO), and sandstone olistostrome beds (SstO) lithotypes. Occasionally, some thin layered bedding was also observed in the olistostromes, indicating some episodic deposition. In most cases, the olistostromes' bodies, as seen in the field, were tectonically tilted due to the Zagros tectonics. Some outcropping olistostrome lithotypes were extensive in the region. A detailed description of all forms of olistostromes observed was provided. In the upper part of the outcrops, the FCO deposits consisted of densely packed lithoclasts supported by a few cm to 25 cm sized carbonate lithoclast. The lithoclasts were often sub-angular to rounded, and more extensive than other lithotype lithoclasts. The lithoclasts were smaller toward the middle and bottom portions of the olistostromes lithotype body (Fig. 3c).

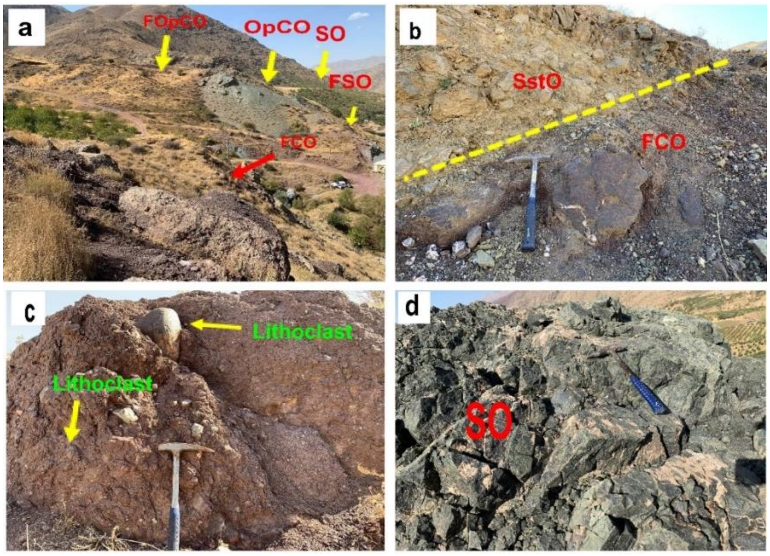

Fig. 3: Field photographs of olistostromes and related rocks in Rayat area: (a) overview of the olistostrome bodies outcrops showing various lithotypes; (b) yellowish to the orange layer of StsO with fine grain matrix and free of lithoclasts over brown FCO; (c) brown FCO body with coarse matrix and the different size of lithoclasts; (d) green SO with size fine grain matrix, rich in quartz and magnetite

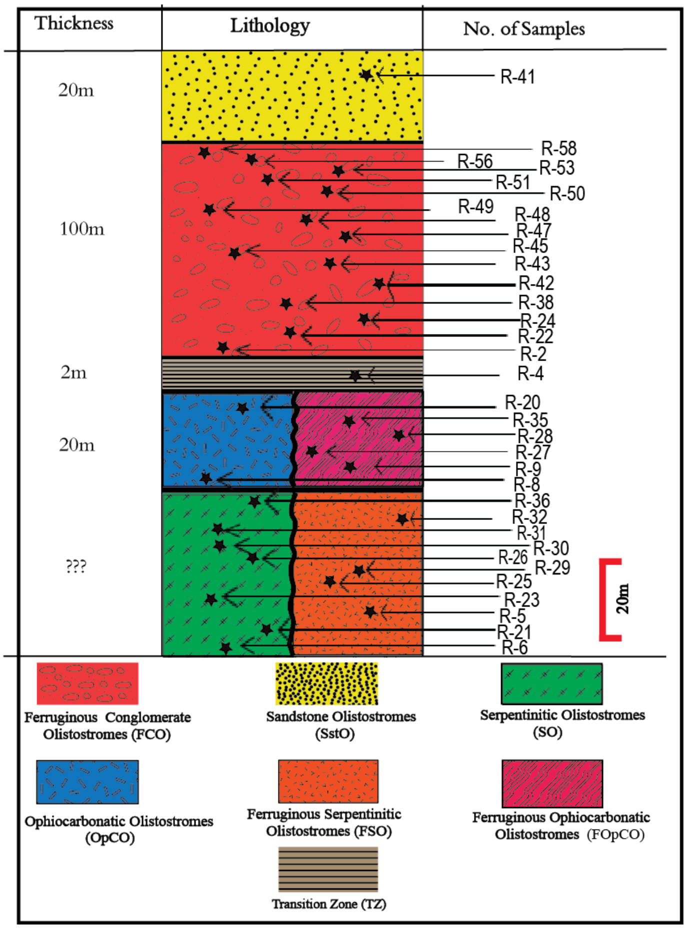

Fig. 4: General lithological column of the Rayat olistostromes lithotypes and succession

4.1.1 Serpentinite Olistostromes (SO) Lithotype

The exposed olistostrome bodies' lower part comprised a fine-grained matrix serpentinite olistostrome (SO) lithotype dominated by serpentinite (Fig. 5a and b). The thickness of SO in the field was about 4-5 m (Fig. 5a). Typically, the serpentinites were massive and green to grey. Furthermore, in several places, the color of observed SO changed to yellowish-blackish (Fig. 5b).

4.1.2 Ophicarbonatic Olistostromes (OpCO) Lithotype

The OpCO lithotype was in contact with SO. It appeared yellowish green (Fig. 5c and d). The serpentinite clasts' sizes ranged from a few mm to several cm and were floated inside carbonate minerals due to the crushing and movement of serpentinites. The clasts were angular and showed a direction due to flow (Fig. 5c).

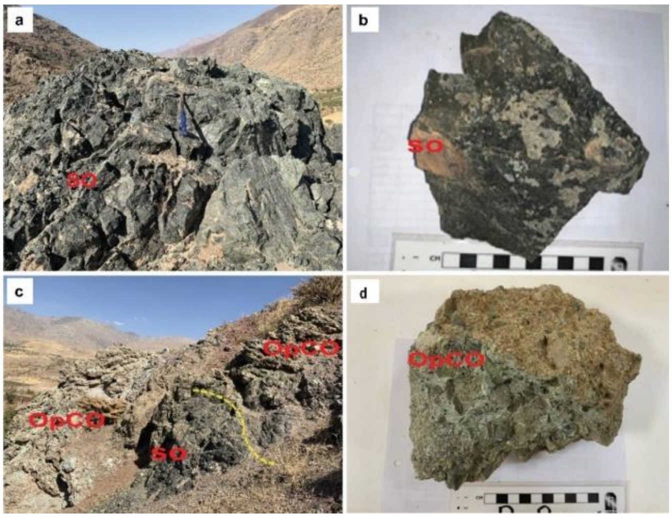

Fig. 5: Field views of O.S. and OpCO in Rayat area: (a) serpentinite olistostrome (SO); (b) fine-grained matrix of SO; (c) gradational contact between SO and OpCO;(d) fine to the coarse-grained matrix of OpCO

4.1.3 Ferruginous Serpentinitic Olistostromes (FSO) Lithotype

Generally, the deposits were brown-reddish in color, and the matrix was fine to coarse-grained (Fig. 6a and b). The bodies had various thicknesses between 4 m to 15 m. Occasionally, the ferruginous serpentinite olistostromes lithotype was re-cemented by iron oxide, such as Hematite (Fig. 6a and b).

4.1.4 Ferrouginous Ophicarbonatic Olistostromes (FOpO) Lithotype

The deposits were typically brown in color, and calcite veins could be seen in the bodies of the study (Fig. 6c and d). The clasts had rounded shapes and ranged in size from a few mm to a few cm (Fig. 6c). There were bodies of varied thicknesses in the range of 4 m to 10 m. The ferruginous ophiocarbonatic olistostrome lithotype bodies were re-cemented by iron oxide, such as Hematite besides the carbonate mineral, the matrix was fine to coarse grain (Fig. 6d).

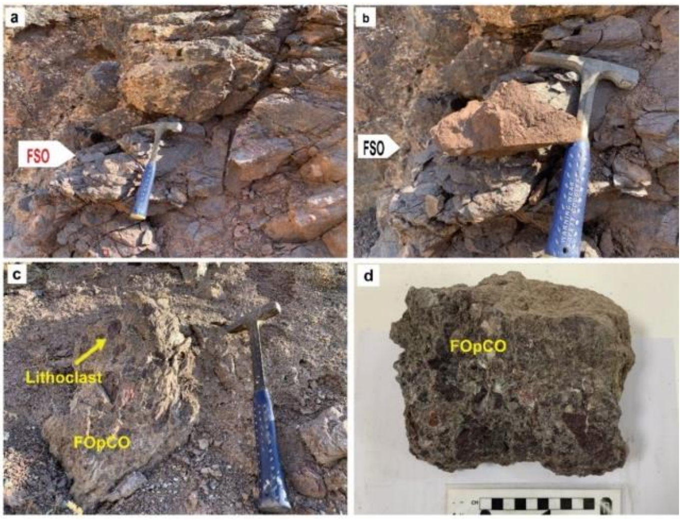

Fig. 6: FSO and FOpCO field views in Rayat area: (a) lithoclasts admixture of various sizes, cemented by ferruginous oxide; the whole body is traversed by vertically oriented calcite veins. Notice that the horizontal serpentinitic lenses within the lithotype indicate both diagenetic alterations from original serpentinites and gradual deposition during the mass flow; (b) sample of FSO lithotype with lenses and serpentinite residual components; (c) various sizes of lithoclasts admixture range from a few mm to a few cm, being cemented by ferruginous; (d) hand sample of brown FSO with fine to the coarse-grained matrix

4.1.5 Transition Zone (TZ)

Between the oxidized zone (FCO) and the mineralization zone (OpCO), this white zone had begun to develop (Fig. 7). This region had a thickness of about 2 m (Fig. 7a). TZ had a color that seems green, but in some places, it had been oxidized, resulting in a brown appearance (Fig.7).

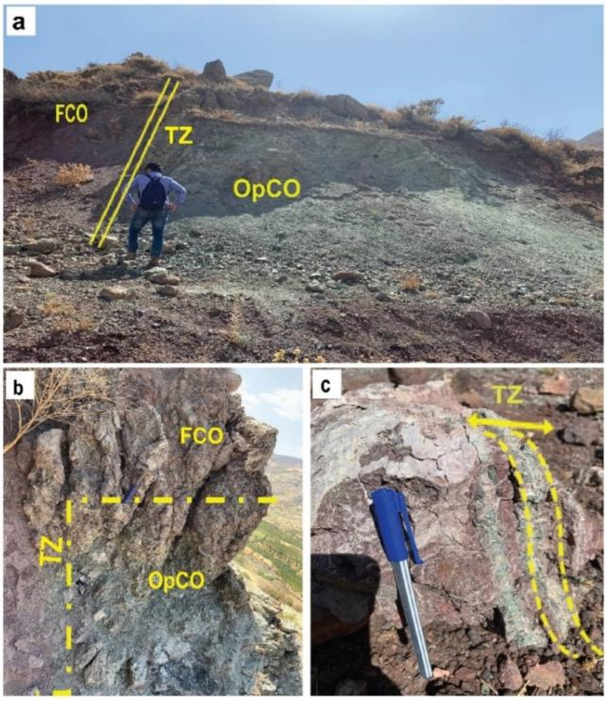

Fig. 7: Field views of the Transition Zone of the study area, (a, b and c) the contact zone between OpCO and FCO

4.1.6. Ferruginous Conglomeratic Olistostromes (FCO) Lithotype

Typically, it appeared brown-reddish with the coarse-grained matrix. At the same time, the lithoclast sizes in the body ranged from a few cm to about 25 cm (Fig. 8c). The bodies were laid on ferruginous serpentinite olistostrome (FSO). The matrix was mainly composed of clay and silt. Additionally, many lithoclasts were angular chert fragments of variable sizes, suggesting rapid turbulent and short transport and sedimentation (Fig. 8c and d). FCO section had direct contact with (SstO). In cross-section, typical ball and pillow structures could be observed.

4.1.7 Sandstone Olistostromes (StsO) Lithotype

The structurally intermediate sandstone matrix olistostrome lied on FCO and appeared near the upper ranges of the study area in Rayat, comprising sandstone enclosing volcanic and sandstone blocks. The layer was yellowish to orange in color (Fig.8e and f). The visible outcrop bed reached 20 m in length, and the bed showed depositional angularity with thickness decreasing to the right, reflecting tectonic unconformity (Fig. 8e). The lithotype showed visible bedding structure, reflecting gradual deposition of ferruginous material during the sediment mass flow (Fig. 8e). The bodies of sandstone olistostrome lithotype were randomly distributed within the bed. This body was free of clasts, fine to coarse grain, and the direction of grain size coursing upward. The blocks were poorly sorted, angular and subangular in shape and set in a sandy matrix (Fig. 8f).

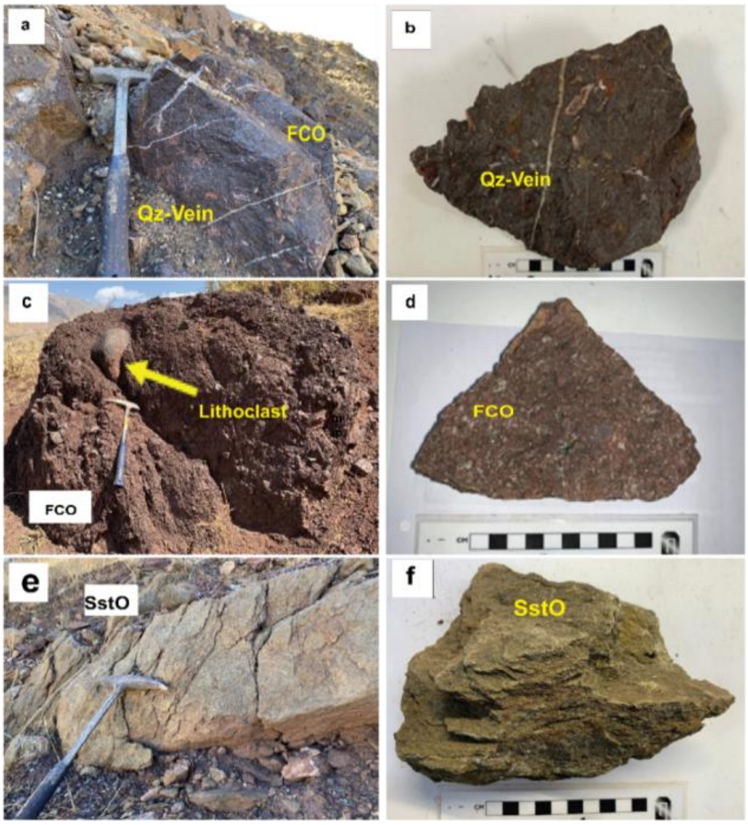

Fig. 8: FCO and SstO field views in Rayat area: (a and b) brown to reddish ball and pillow structures with quartz vein in FCO, (c) various sizes of clasts in FCO coarse grain matrix, (d) brown and coarse-grained matrix rock sample of FCO, (e) bedded SstO showing depositional angularity with thicknesses decreasing to the right, (f) yellow to orange and fine-grained matrix with rock sample

4.2 Mineralogy and Petrography

Detailed optical microscopy and XRD study are presented in (Table 1, Figs. 9, 11,12,13,14,15 and 16), which are used to identify the mineral characteristics of the different lithotypes of the olistostromes at the Rayat area.

Table 1: **Semiquantitative XRD results of the different facies (lithotype) of the olistostromes (M: main, m: minor, T: trace)**

Body associated rocks				Mineral[1]											
Rock	**Ab**	**Cal**	**Ctl**	**Gr**	**Cpx**	**Dol**	**Antig**	**Hem**	**Liz**	**Mag**	**Chro**	**Zeo**	**Qz**	**Bio**	**Tlc**
OpCO		M							M						
FCO		m						T					M		
SO			M				M		M	T					m
FOpCO		m				M		m	M			T			
FOpO		M		T	m							T	T		
FSO					T			M			m	T			
FCO								T			T	M	T		
FCO	m							T			T	M			
.Z.	M	m						T					M		

[1]: Ab: albite, Anti: Antigorite, Cal: calcite, Chr: chromite, Ctl: chrysotile, Cpx: clinopyroxene, Dol: dolomite, Hem: Hematite, Liz: lizardite, Mag: magnetite, Qz: quartz, Tlc: talc, and Zeo: Zeolite

4.2.1 Serpentinite Olistostromes (SO) Lithotype

The serpentinite olistostromes lithotype were rich in lizardite, antigorite, calcite, quartz, and talc as minor mineral (Table 1, and Figs. 9 (a, b, c) and 15), generally showing mesh texture after olivine and pyroxene (Fig. 9a).

Olivine and pyroxene were common minerals with a minor amount of Spinel, magnetite, and Hematite. Here, the serpentines mainly replaced olivine and pyroxene in fractures and along cleavage and had a mesh texture (Fig. 9a). Due to recrystallization in the cavities, quartz was formed as a mega crystal, and the texture of the case became druzy (Fig.9b). Individual grains of Cr-spinel and chromite exhibit skeletal texture were broken and subjected to brecciation. The stockwork structure, generated by the crosscutting of calcite and serpentinite mineral veins, was also shown by optical microscopy of thin parts (Fig. 9c). They existed as euhedral to subhedral dispersed crystals. Spinel had skeletal texture (Fig. 9d). Serpentines filled fractures between primary minerals, such as olivine and pyroxene; while in some parts, they had been entirely replaced by minerals.

4.2.2 Ophiocarbonatic Olistostromes (OpCO)

The mineralogical study showed that the OpCO lithotype was rich in lizardite and calcite (Table 1 and Fig. 9e). After that, olivine and pyroxene displayed a mesh texture (Fig. 9a). The matrix of OpCO was calcite (Figs. 9 (e) and 16). Each Cr-spinel and chromite grains had a skeletal texture, were fractured and undergone brecciation. Spinel had a skeletal texture and was formed as euhedral to subhedral scattered crystals (Fig. 9f). Elemental mapping of the OpCO samples (Fig. 10a) by SEM-EDS showed that the sample contained phases rich in Fe (Fig. 10b), inside grains of serpentines, which were rich in Si and Mg (Fig. 10 c and d). The large grains of serpentines were enclosed by a matrix rich in calcite (Fig. 10e). This texture showed the formation of ophiocarbonatic rocks.

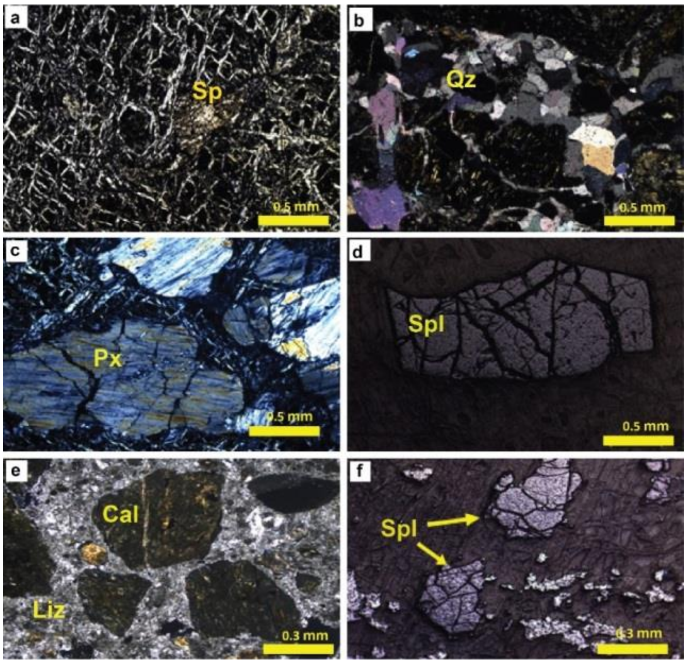

Fig. 9: photomicrographs showing mineralogical composition and microstructure of the Rayat SO and OpCO: (a) mesh texture of serpentinite, (b) quartz grains as mega crystal with druzy texture, (c) calcite veins displayed in variable sizes, (d) variable sizes of subhedral grains of spinal in the matrix of serpentine, (e) different sizes of calcite veins, and (f) variable sizes of subhedral grains of Cr-spinel mineral subjected to brecciation with skeletal texture Quartz (Qz), Serpentine (Sp), Pyroxene (Px), (Calcite (Cal), (Spinal (Spl), and Lizardite (Liz)

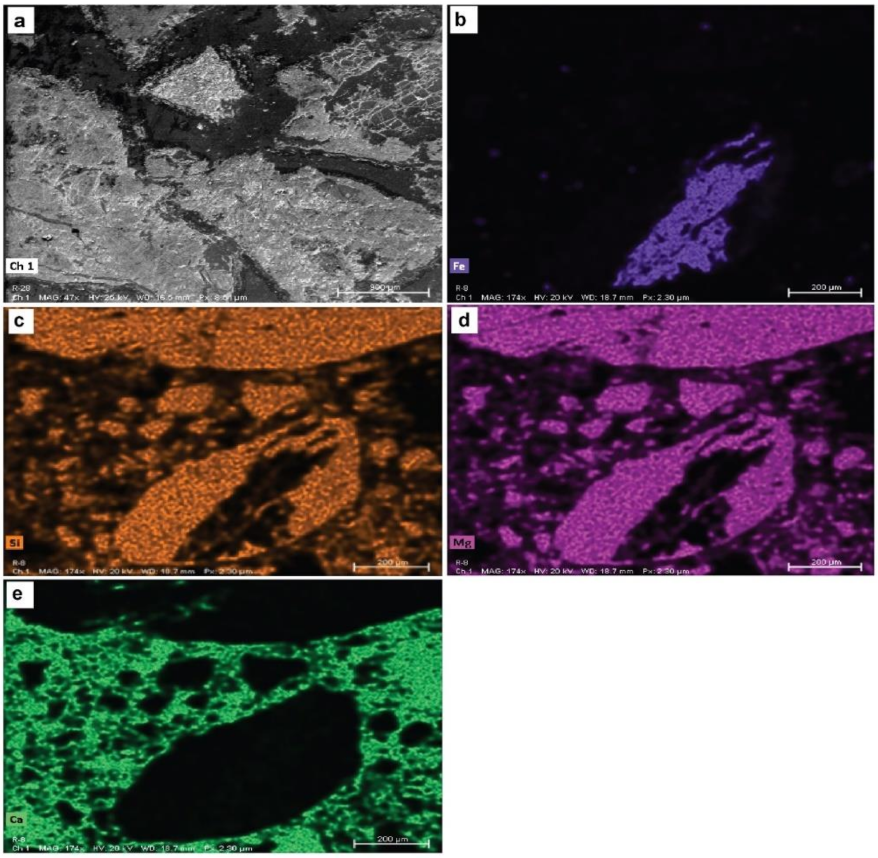

Fig. 10: Photographs of SEM images mapping of b) Fe, c) Si, d) Mg, e) Ca, opiocarbonatic olistostrome distributed (R-8) Fe-clearly dispersed and Si-Mg-Ca rich zone, appearing randomly scattered regions with calcite green background of rocks

4.2.3 Ferruginous Serpentinite Olistostromes (FSO) Lithotype

The ferruginous serpentinite olistostrome (FSO) was mainly composed of serpentine, quartz, and calcite, with a minor amount of albite and Hematite (Table 1, and Fig. 11a and b). Calcite was present as secondary veins cutting quartz (Fig. 11a). The quartz grains were generally sub-rounded to rounded in shape with various grains sized and coarse-grained calcite (Fig. 11a and b). The matrix was predominantly composed of Hematite (Fig. 11c). Other minerals were Cr-spinel; the Cr-spinels had subhedral and euhedral, a skeletal form that appeared like a skeleton under the microscope (Fig. 11d).

4.2.4 Ferruginous Ophicarbonatic Olistostromes (FOpCO) Lithotype

The FOpCO lithotype was mainly composed of calcite and dolomite as major minerals and zeolite as a race mineral (Table 1, and Fig. 11e). Hematite was present in the body as a matrix (Fig. 11f). Opaque minerals, such as Cr-spinel, was observed under the microscope, which had an anhedral to skeletal form (Fig. 11d).

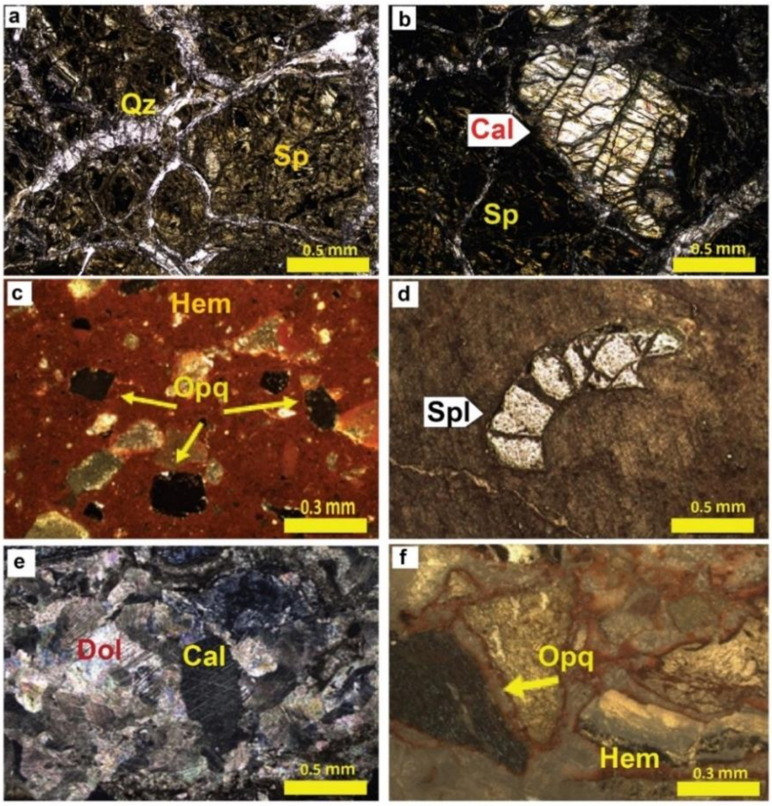

Fig. 11: Photomicrographs showing mineralogical composition and microstructure of Rayat FSO lithotype, (a) veins of calcite cutting quartz through calcite matrix with the druzy texture of quartz, (b) variable sizes of quartz, plagioclase, and albite, (c) hematite as a matrix, (d) disseminated Cr-spinel with mostly skeletal texture and subhedral shape, (e) calcite and dolomite, and (f) hematite dominated
Quartz (Qz), Calcite (Cal), Hematite (Hem), Spinal (Spl), Dolomite (Dol)

4.2.5 Transition Zone (TZ)

Transition zone mineralogy was dominated by quartz, calcite, albite (Fig.12a and b) and a minor amount of Cr-spinel. Hematite was the other frequent mineral in this zone (Table 1). The calcite crystals were mostly subhedral or euhedral and angular as accessory minerals. They could be observed as a single component (Fig. 12b). Hematite was the primary content of the matrix (Fig. 12d).

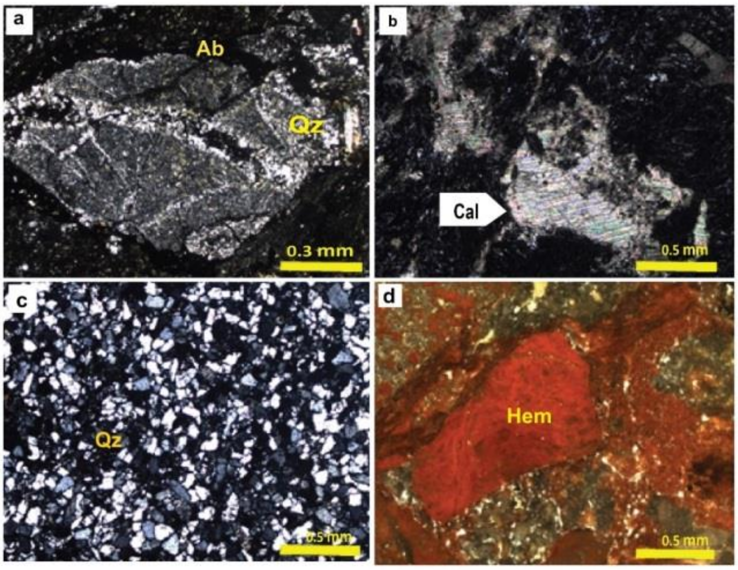

Fig. 12: Photomicrographs of TZ and FCO samples of Rayat area, a) calcite veins and quartz, (b) calcite vein, (c) clasts composed of quartz grain with the druzy texture of quartz, and (d) hematite as a matrix
Albite (Ab), (Quartz (Qz), Calcite (Cal), Hematite (Hem)

4.2.6 Ferruginous Conglomeratic Olistostromes (FCO) Lithotype

FCO lithotype was mainly composed of quartz as major mineral and minor amounts of Hematite, magnetite and Spinel (Table 1). Quartz was formed with different sizes, from fine to coarse grains with subhedral shapes. The grains were angular in most cases (Fig. 13a and b). Sometimes remnant of fossils was present and replaced by quartz (Fig. 13b). Spinel was the other subhedral mineral in this unit with different sizes (Fig. 13c). Hematite (very fine-grained) was mainly formed by the matrix of rocks (Fig. 13c and d). Some remnants of fossils (foraminifera) could be seen in the samples as well preserved and replaced by Hematite (Fig. 13d). Magnetite showed a rounded shape with different sizes up to 0.3 mm (Fig. 13e and f).

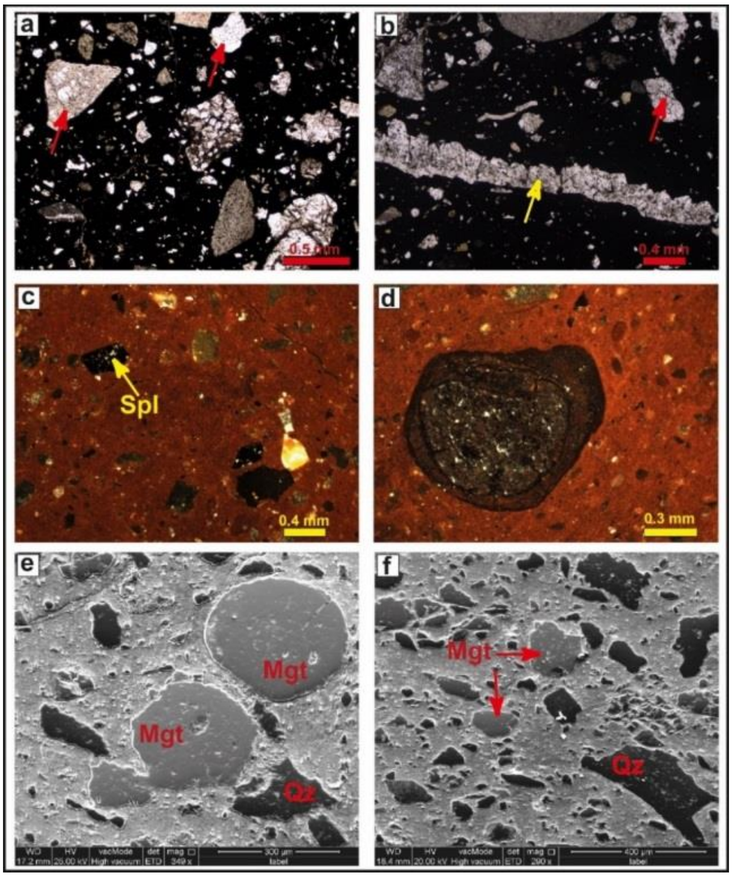

Fig. 13: Photomicrographs showing mineralogical composition and microstructural characteristics of the ferruginous conglomerate olistostromes of the Rayat-Choman area, (a-c) presence of abundant grains of quartz (red and yellow arrows) of different sizes, which are enclosed by an iron oxide (Hematite) matrix. In some places, fossils are replaced by silica (fig. 14 b, yellow arrow), (b-c) presence of Hematite as a matrix (orange colors), and Spinel formed as subhedral crystals, (e-f) roundish grains of magnetite of different sizes represent the movement of this mineral from the source (Mgt: magnetite, Qz: quartz, and Spl: spinel)

4.2.7 Sandston Olistostrom (SstO) Lithotype

The SstO lithotype was rich in fossils, mainly different types of foraminifera and algae. The fossils were replaced by quartz and calcite. In some cases, the cells were replaced by framboidal pyrites (Fig. 14a, b, and c). Feldspars, which are subhedral, were mostly of plagioclase type in thin sections. Most plagioclase appeared in the coarse-grained sandstones of the sandstone olistostrome lithotype.

The petrographical examination of thin sections indicated that the samples were primarily pure sandstone, for which different types of fossils had been recognized. Carbonate lithoclasts in SstO showed abundant intact microfossils of green alga dasyclads neomeris, trinocladus perplexus elliott, sponges' fragments, corals, and foraminifera (miliolid, and nummulites, opercoulina ammonida) (Fig. 14a, b, and c). These daysclad algae were typical of the Paleocene-Eocene period in Kurdistan, pertaining probably to the Sinjar formation equivalent. The bioclasts were significant indicators of the dating and formation age of the olistostromes in the Choman area, hence paleotectonic interpretation. The minerals fragments included quartz grains, feldspar, and pyrite spots (Fig. 14d).

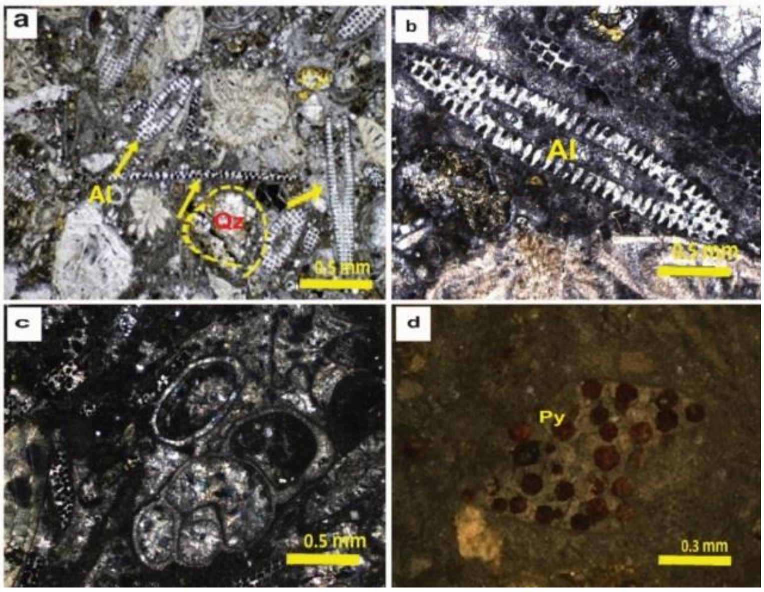

Fig. 14: Photomicrographs of SstO samples of the Rayat olistostromes: (a, b, and c) carbonate lithoclasts in SstO show abundant intact microfossils of green algae Dasyclads Neomeris, Trinocladus, Perplexus Elliott, sponges' fragments, corals and foraminifera (Miliolids, and Nummulites, Opercoulina), and (d) shows pyritization of fossil cavities (rounded black) probably replacing original organic content. Quartz crystals (red spots) are also present Quartz (Q.Z.), Algae (Al), Pyrite (Py)

4.3 Mineral Chemistry

According to SEM-EDS results, the serpentines of SO were composed of Mg (ave.40.54 wt.% MgO), and Si (ave. 44.24 wt.% SiO_2). Moreover, the serpentines had low Ni (ave. 0.09 wt. %) and Cr content (ave. 0.35 wt. % Cr_2O_3). In the sample of ophiocarbonatic olistostromes (OpCO), the average content value of Ni was observed to be 0.35 in serpentine mineral wt. %, and Cr was observed to be 0.36 wt. % in magnetite minerals. Whereas the average concentration of K_2O was determined in serpentinite olistostromes (SO) as 0.01 wt. %. Additionally, the concentrations of both Fe_2O_3 and MgO were rather high, as 80.5 wt. % in manatite mineral and 40.26 wt. % in serpentine mineral on average, respectively. Chromite mineral from R-6 showed a high amount of $Cr_2O_{3,}$ which was 36.04 wt. % (Table 2).

Sample R-21 from ferruginous serpentinite olistostromes (FSO) was primarily composed of serpentine with typical 44.66 wt.% of SiO_2 and 33.49 wt.% of MgO. Besides, Fe_2O_3 and Al_2O_3 displayed low concentration in serpentine mineral. The other phase was diopside, with ave. 0.00 wt.% of MgO, 1.31 wt.% of Al_2O_3 in diopside mineral and with a high concentration of CaO 51.62 wt. % in diopside (Table. 2). However, the concentrations of Ni and Cr2O3 were low in diopside minerals, which were (ave. 0.2 wt. % and 0.00 and 0.29 wt. %) in serpentine.

The composition of sample R-8 from the ophiocarbonatic olistostromes (OpCO) was primarily made up of calcite, which had an average of 54.81 wt.% of CaO and 15.89 wt.% MgO. However, pyroxene had an average of 44.98 wt.% of SiO_2 and 38.66 wt.% MgO. Hematite had a high amount of Fe_2O_3 with an average of 85.41 wt.%. Nevertheless, the amount of Ni was low in calcite (Table 2).

Sample R-28 from ferruginous ohiocarbonatic olistostromes (FOpCO) was typically composed of calcite with the average of 84.88 wt.% of CaO, ave.2.14 wt.% of MgO and 0.01 wt.% of K_2O. Whereas it displayed a high amount of SiO_2 (57.12 wt.% on Avg.) and MgO (31.32 wt. % on Avg.) in serpentine minerals. The concentration of Fe_2O_3 was highest at 92.2 wt. %, in hematite mineral. The concentration of Cr_2O_3 was high in chromite mineral (40.51 wt.%), while it contained unknown mineral with an average of 35.23 wt.% of SiO_2, 20.06 wt.% of MgO. The concentration of K_2O was highest (about 24.38 wt.%) in unknown mineral (Table 2).

The FCO sample (R-43) contained quartz, chromite, magnetite, hematite, and chlorite. The quartz showed high amount of SiO_2 (about 90.50 wt.% on avg) and comprised a significant quantity of Fe_2O_3, which was 91.69 wt.% in magnetite mineral and contained 69.29 wt.% of iron.

Table 2: SEM-EDS results of mineral composition of Rayat olistostromes lithotypes (Un.Min.: Unknown Mineral)

Sample	Mineral	SiO_2	MgO	Fe_2O_3	Al_2O_3	K_2O	TiO_2	CaO	Cr_2O_3	MnO	Na_2O	Sc	V	Co	Ni	Cu	Zn	As	Rb	Sr	Y	Mo	Cl
R41 (SstO)	Chlorite	37.52	14.84	18.96	16.30	0.43	0.39	1.85	0.31	0.13	1.95	0.02	0.02	0.07	0.19	0.02	0.38	0.04	1.59	0.06	0.07	3.53	
	Calcite	0.74	1.82	0.47	1.04	0.02	0.08	86.72	0.01	0.20	1.16	0.21	0.01	0.02	0.07	0.07	0.57	0.00	1.49	0.16	0.18	3.81	
	Feldspar	50.55	4.84	6.19	16.03	1.36	4.77	4.66	0.07	0.12	5.44	0.02	0.02	0.05	0.06	0.03	0.19	0.00	0.69	0.03	0.11	3.37	
	Quartz	92.42	0.00	0.04	0.47	0.01	0.00	0.22	0.00	0.00	0.00	0.05	0.03	0.01	0.02	0.00	0.28	0.00	0.75	0.00	0.13	4.29	
R43 (FCO)	Quartz	90.59	0.12	1.93	1.20	0.39	0.02	0.02	0.09	0.01	0.15	0.01	0.01	0.04	0.06	0.01	0.41	0.00	0.00	0.00	0.00	3.50	
	Chromite	0.00	10.55	16.14	19.08	0.02	0.06	0.06	44.79	0.79	1.12	0.02	0.13	0.26	0.11	0.05	0.26	0.00	2.15	0.00	0.00	3.07	
	Hematite	14.36	1.46	69.29	4.60	1.21	0.18	0.11	1.52	0.09	0.98	0.01	0.08	0.73	0.28	0.11	0.03	0.09	0.83	0.00	0.05	2.63	
	Magnetite	0.17	0.01	91.69	0.67	0.00	0.23	0.11	1.54	0.22	0.00	0.02	0.02	1.11	0.31	0.25	0.06	0.00	0.65	0.00	0.16	1.84	
	Chlorite	18.53	5.80	52.03	12.66	1.64	0.19	0.21	1.05	0.28	0.99	0.00	0.07	0.55	1.59	0.09	0.02	0.09	0.57	0.00	0.22	1.98	
R28 (FOpCO)	Chromite	0.00	10.75	17.89	23.05	0.01	0.00	0.13	40.51	0.22	0.76	0.01	0.10	0.18	0.18	0.04	0.51	0.07	1.37	0.36	0.00	2.58	
	Serpentine	57.12	31.32	0.87	1.69	0.02	0.03	0.83	0.07	0.10	0.70	0.05	0.02	0.04	0.32	0.03	0.26	0.01	1.29	0.22	0.24	4.10	
	Calcite	0.43	2.14	0.24	0.95	0.01	0.03	84.88	0.03	1.47	1.56	0.00	0.01	0.01	0.06	0.00	0.26	0.00	2.32	0.25	0.00	3.63	
	Hematite	0.13	1.00	92.21	1.18	0.01	0.09	0.11	0.01	0.05	1.48	0.03	0.02	0.40	0.05	0.01	0.34	0.00	1.24	0.17	0.11		
	Un.Min.	35.23	20.06			24.38					3.18												16.28
R8 (OpCO)	Hematite	0.11	1.60	85.41	2.31	0.00	0.11	0.10	0.06	0.10	1.57	0.06	0.01	0.55	0.41	0.12	0.05	0.00	0.00	2.79	0.00	3.49	
	chlorite	36.52	36.52	16.74	0.94	0.04	0.01	0.23	0.00	0.23	0.86	0.00	0.00	0.12	0.37	0.15	0.64	0.00	1.25	0.00	0.00	3.54	
	Pyroxene	44.98	38.66	5.20	1.91	0.00	0.00	0.14	0.26	0.00	0.53	0.04	0.02	0.13	0.27	0.03	0.63	0.00	1.80	0.00	0.00	3.72	
	Calcite	15.07	15.89	4.05	1.91	0.01	0.00	54.81	0.08	0.00	0.96	0.13	0.00	0.00	0.10	0.00	0.86	0.00	0.00	0.43	0.00	3.94	
	Serpentine	39.89	36.12	6.19	1.67	0.01	0.01	0.35	0.08	0.13	0.67	0.01	0.01	0.05	0.29	0.02	0.22	0.00	1.73	0.00	0.00	1.96	
R21 (FSO)	Serpentine	44.66	33.49	7.36	2.63	0.03	0.02	0.18	0.29	0.09	0.59	0.01	0.01	0.08	0.28	0.03	0.37	0.08	0.63	0.21	0.07	3.99	
	Diopside	0.00	31.34	0.06	1.31	0.04	0.00	51.62	0.00	0.12	1.37	0.00	0.03	0.10	0.02	0.00	0.98	0.00	3.69	0.00	0.00	5.71	
	Chlorite	26.67	18.56	44.69	1.41	0.00	0.00	0.00	0.05	0.14	1.62	0.02	0.06	0.36	0.20	0.00	0.57	0.00	0.76	0.00	0.52	3.38	
R6 (SO)	Serpentine	42.26	40.34	6.35	1.57	0.00	0.04	0.09	0.35	0.11	0.80	0.02	0.03	0.05	0.35	0.06	0.35	0.02	0.92	0.16	0.05	4.38	
	Magnetite	3.15	5.21	80.51	1.71	0.01	0.02	0.17	0.36	0.07	2.35	0.01	0.02	0.68	0.52	0.15	0.00	0.00	0.27	0.24	0.10	3.74	
	Chromite	3.56	13.74	16.99	22.05	0.01	0.04	0.03	36.04	0.34	1.22	0.01	0.09	0.22	0.20	0.01	0.64	0.01	0.49	0.00	0.23	2.96	

Oxide in hematite mineral contained the highest amount of Cr_2O_3 44.79 wt.% in chromite mineral (Table 2).

Sample R-41 was taken from sandstone olistostromes (SstO) and was mostly comprised of quartz. Its concentrations were in quartz mineral as follows: the highest amount was recorded for SiO_2 as 92.42 wt.%, 0.00 wt.% for MgO, 0.47 wt.% for Al_2O_3 and 0.04 wt.% for Fe_2O_3 on average. The sample was also made of calcite and contained 86.72 wt.% of CaO in calcite mineral. In addition, it contained an average of 16.03 wt. % of Al_2O_3 in feldspar mineral and 5.44 wt. % of Na_2O in feldspar mineral (Table 2).

Nevertheless, the SEM-EDS result indicated that the high concentrations of Fe and Si were in a silicate mineral, while Mg and Ca demonstrated high concentrations in carbonate mineral. The other types of olistostromes, such as SO, OpCO, and FSO, were moderately rich in carbonate and silicate minerals.

4.4 Fossil Bacteriomorphs

The SEM study of the sample slabs, chips, and thin sections from the iron-rich conglomerate unit showed well-preserved, rich, and matrix-embedded microbial assemblages. Remnants of microbial mats and EPS biofilms were also present. Most of the bacteriomorphs were densely encrusted with iron silicates. The substrates and the microbial-cellular contents were all mineralized and well-embedded in the substrate. The types of bacteriomorphs included mineralized fossil bacteria and cellular material (Fig. 15a), undifferentiated microbial filaments (cyanobacteria and/or fungi) (Fig. 15b), filamentous, cellular and bacterial forms (Fig. 15c), and cellular material and a few filamentous, rod and coccoid bacterial forms (Fig. 15d). Some forms were probably pertaining to algal material (center of photo). A probable remnant of a microbial mat showing a soft layer pressure impression is shown in Figure 15d. The mineralization chemistry made of nano-size crystals mainly included Fe and Si, suggesting elements' mobility and precipitation during a hydrothermal event. The bacteria-iron interactions that could produce iron precipitation and deposits were well-known in the literature [30-32]. The general interaction assumed the oxidation of dissolved Fe (II) via abiotic oxidation by cyanobacterial-produced O_2 and biotic oxidation by chemolithotrophic bacteria [33].

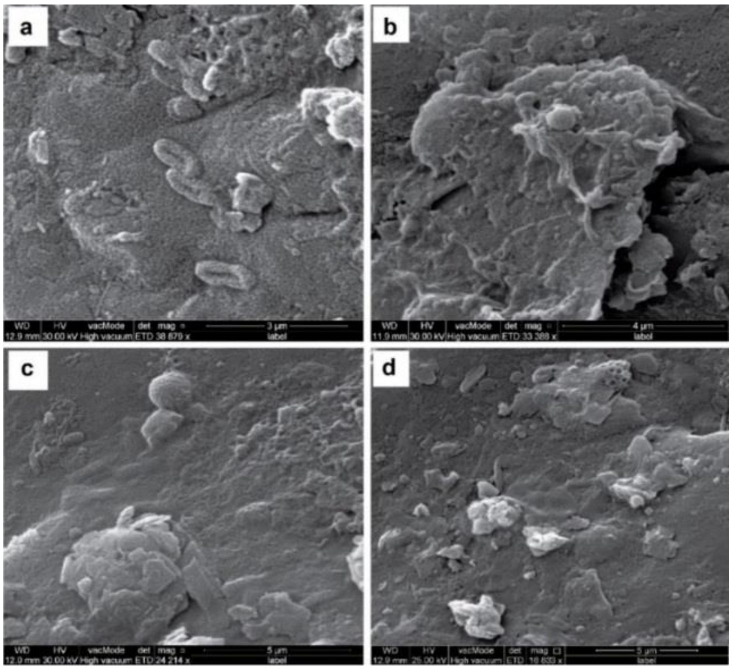

Fig. 15: SEM micrographs of rock chip from sample R-24 showing extensive microbes-mineral interaction on the rock substrate. The substrates, as well as the microbial-cellular contents, are all mineralized and well-embedded in the substrate. (a) Mineralized fossil bacteria and cellular material, (b) undifferentiated microbial filaments (cyanobacteria Fungi), (c) filamentous, cellular and bacterial forms, and (d) cellular material and few filamentous, rod and coccoid bacterial forms

4.5. Whole Rock Geochemistry

Table 3 shows the geochemical analysis results of the olistostromes lithotype in the Rayat area. The serpentinitic olistostromes (SO) had high concentration of SiO_2 (0.16-47.13 w t.%), whereas Fe_2O_3 content was in the range of 5.43- 9.7 wt.%. and MgO in the range of 22.61-35.11 wt.%. Serpentinite olistostromes showed that the highest concentration of MgO was 35.11 wt.%, as compared to other types of olistostromes lithotypes.

The ophiocarbonatic serpentinitic olistostromes (OpCO) had the highest concentration of CaO (24.47-27.72 wt.%), whereas its silica content was in the range of 19.17-22.38 wt.%; it showed the high concentration of Fe_2O_3 as 5.28 wt.%, and Mg 20.25 wt.%. Al_2O_3 had a low concentration in the range of

0.35-0.46 wt%. All the other major oxides showed concentration below <1 wt.% in all horizons.

The ferruginous serpentinite olistostromes (FSO) were rich in SiO_2 (31.81-86.05 wt.%), with an average of Fe_2O_3 concentration of 8.48 wt.%. While Al_2O_3 had a concentration in the range of 0.12-6.68 wt.%.

The ferruginous ophiocarbonatic olistostromes (FOpCO) was rich in SiO2 in the range of 24.45-37.88 wt.%. While Fe_2O_3 had a concentration in the range 3.83-7.72 wt.%. Its MgO concentration was 18.53 wt.% on average. The transition zone (TZ) was rich in SiO_2 (66.07 wt%) with an average Fe_2O_3 concentration of 12.73 wt.% (Table. 3). Ferruginous ophiocarbonatic olistostromes (FOpCO) were concentrated in SiO_2 and CaO.

The studied ferruginous conglomerate olistostromes (FCO) were rich in SiO2 (43.35-74.23 wt.%), displaying also elevated concentrations in MgO and Al_2O_3. Ferruginous conglomerate olistostromes (FCO) lithotype was enriched in iron oxide with the highest average of 42.55%. wt (Table 3). The ferruginous conglomerate olistostromes (FCO) were enriched in silicate minerals, such as quartz (SiO_2). In addition, the quantity of CaO was low in the rock formation (Table 3).

The sandstone olistostromes studied (SstO) were rich in SiO_2, which was 48.93 wt.%. While Fe_2O_3 concentration was 27.73 wt.% (Table 3). Silica appeared mostly in the major mineral quartz in lithotypes. The presence of quartz-veins suggested subsequent abundant mineral. Sandstone olistostromes (SstO) were enriched in silicate minerals, such as Quartz (SiO_2), and carbonate minerals, such as calcite.

Potassium and sodium concentrations were generally low in all olistostromes lithotypes, consistent with their development. Only the FCO samples including quartz with the amount of K_2O (3.09 wt %) and Cr (8,495 mg/kg) were correlated, although spinel was not present. The superior value of Fe_2O_3 could be the result of the existence of spinel, magnetite and its supergene-related iron oxide.

Concerning the composition of minor and Rare Earth Elements (REE), chromium, nickel and cobalt were abundant in all lithotypes (Table 3). FCO had the highest amount of Ni and Cr (5,816 mg/kg and 8,495 mg/kg, respectively). Nickel concentrations were lower in SstO (507 mg/kg), Cobalt concentrations in the top of the horizon (FCO) were 328 mg/kg, and in serpentinite and olistostromes were lower within the range of 62.5-112.1 mg/kg. The average concentration of the Cr_2O_3 in (SO) was 2303 mg/kg. The concentration of rare elements in most samples was relatively low in all of the examined lithologies, being quite depleted and revealing a comparable average to that of the metasomatized mantle (Zhou et al., 2004; Tsikouras et al., 2006) (Table 3).

Table 3: Geochemical results of the studied olistostromes samples and associated lithologies of the Rayat region

Sample		**R-06**	**R-21**	**R-26**	**R-30**	**R23**	**R-31**	**R-36**	**R-05**	**R-25**	**R-29**	**R-32**	**R-08**	**R-20**	**R-09**	**R-27**	**R-28**	**R-35**
Lith.a		**SO**	**SO**	**SO**	**SO**	**SO**	**SO**	**SO**	**FSO**	**FSO**	**FSO**	**FSO**	**OpO**	**OpO**	**F-OpO**	**F-OpO**	**F-OpO**	**F-OpO**
wt.%	DL																	
Al_2O_3	0.05	0.47	0.26	0.33	0.3	0.37	0.67	3.29	6.67	0.53	0.51	0.12	0.35	0.46	1.26	0.94	0.81	0.12
CaO	0.05	0.46	5.4	0.34	19.89	0.67	2.69	4.93	11.03	0.15	11.31	9.51	24.5	27.72	31	9.44	19.71	9.95
Fe_2O_3	0.05	8.46	6.99	9.7	5.43	9.59	8.76	7.23	8.01	14.5	5.86	5.91	4.89	5.28	3.83	7,72	6.15	5.94
K_2O	0.05	0.05	0.05	0.05	0.05	0.05	0.05	0.29	1.43	0.05	0.05	0.05	0.05	0.05	0.05	0.05	0.05	0.05
MgO	0.05	35.11	30.9	35.3	22.61	33.4	34.59	22.9	3.51	25.07	27.74	27.2	20.3	17.74	10.31	25.65	19.63	29.6
MnO	0.05	0.11	0.16	0.12	0.1	0.08	0.18	0.09	0.14	0.23	0.11	0.16	0.07	0.07	0.07	0.31	0.29	0.13
Na_2O	0.05	0.06	0.16	0.05	0.05	0.05		0.71	1.05	0.05	0.05	0.05	0.05	0.05	0.18	0.05	0.05	0.05
P_2O_5	0.05	0.05	0.16	0.05	0.05	0.05	0.05	0.08	0.08	0.05	0.05	0.05	0.05	0.05	0.05	0.05	0.05	0.05
SiO_2	0.05	39.72	0.16	39.1	25.82	41.2	35.73	47.1	56.45	53.33	31.81	40.9	22.4	19.17	24.45	37.88	28.91	34
TiO_2	0.05	0.05	0.16	0.05	0.05	0.05	0.05	0.37	0.62	0.05	0.05	0.05	0.05	0.05	0.11	0.05	0.05	0.05
LOI	0.05	14.75	0.16	14.2	25.37	13.9	15.9	12.4	10.62	4.93	22.18	15.7	27.1	29.08	28.02	17.33	23.95	19.77
Total		99.14	44.6	99.5	99.52	99.8	99.45	99.4	99.61	99.54	99.52	99.5	99.6	99.52	99.23	91.55	99.45	99.51
mg/kg	DL																	
As	0.1	<0.1	3.3	1	2	2.7	0.5	2.3	1.3	1.4	2.3	<0.1	1.4	1.2	<0.1	0.8	0.1	0.8
Ba	1	<1	<1	<1	18	9	<1	39	74	<1	8	<1	<1	1	1	<1	<1	<1
Be	0.2	<0.2	<0.2	<0.2	<0.2	<0.2	<0.2	0.2	0.7	<0.2	<0.2	<0.2	<0.2	<0.2	<0.2	<0.2	<0.2	<0.2
Ce	0.5	<1	<1	<1	<1	<1	<1	3	20	<1	<1	<1	<1	<1	<1	<1	<1	<1
Co	1	104.9	86.6	112	62.5	106	128.1	101	63.5	194.5	63.9	73.3	57	58	48.2	100.7	72.7	71.7
Cr	1	1773	2218	1874	954	3124	3793	1753	1194	5153	10.34	1314	798	1191	752	2189	1507	1433
Cs	0.5	<0.5	0.7	<0.5	<0.5	1	<0.5	3.1	3.7	<0.5	0.5	<0.5	<0.5	<0.5	0.5	0.7	0.7	0.6
Cu	1	4	28	3	59	7	51	14	23	42	9	14	5	3	12	9	25	3
Dy	0.02	0.09	0.1	0-.1	0.1	0.08	0.08	0.95	2.14	0.23	0.09	0.1	0.1	0.13	0.39	0.23	0.25	0.1
Er	0.05	0.13	0.13	0.12	0.14	0.12	0.15	0.55	1.22	0.24	0.14	0.12	0.16	0.14	0.32	0.25	0.25	0.14
Eu	0.1	<0.1	<0.1	<0.1	<0.1	<0.1	<0.1	0.22	0.62	<0.1	<0.1	<0.1	<0.1	<0.1	<0.1	<0.1	<0.1	<0.1
Gd	0.05	<0.05	<0.05	<0.05	<0.05	<0.05	<0.05	0.74	2.04	<0.05	<0.05	<0.05	<0.05	<0.05	<0.05	<0.05	<0.05	<0.05
Hf	0.5	<0.5	<0.5	<0.5	<0.5	<0.5	<0.5	<0.5	0.78	<0.5	<0.5	<0.5	<0.5	<0.5	<0.5	<0.5	<0.5	<0.5
La	1	<1	<1	<1	<1	<1	<1	3	11	<1	<1	<1	<1	<1	<1	<1	<1	<1
Li	1	<1	7	<1	<1	3	<1	<1	13	<1	<1	<1	<1	<1	<1	<1	<1	<1
Lu	0.1	<0.1	<0.1	<0.1	<0.1	<0.1	<0.1	<0.1	0.14	<0.1	<0.1	<0.1	<0.1	<0.1	<0.1	<0.1	<0.1	<0.1
Mo	0.1	1	<0.1	<0.1	<0.1	2	2	9	6	1	<0.1	<0.1	<0.1	<0.1	1	<0.1	1	<0.1

Nb	1	<1	<1	<1	<1	<1	<1	2	4.3	<1	<1	<1	<1	<1	<1	<1	<1	<1
Nd	0.5	<0.5	<0.5	<0.5	<0.5	<0.5	<0.5	3.2	9.6	<0.5	<0.5	<0.5	<0.5	<0.5	<0.5	<0.5	<0.5	<0.5
Ni	1	2178	1697	2239	1356	2117	2296	1886	1074	3907	1362	1776	1141	1165	963	2071	1548	1457
P	10	49	48	42	RF	42	44	253	303	66	51	50	112	103	129	68	86	47
Pb	1	<1	<1	<1	<1	<1	<1	<1	1	<1	<1	<1	<1	<1	<1	<1	<1	<1
Pr	0.05	<0.05	<0.05	<0.05	<0.05	<0.05	<0.05	0.7	2.23	<0.05	<0.05	<0.05	<0.05	<0.05	<0.05	<0.05	<0.05	<0.05
Rb	1	2	2	2	2	2	2	9	33	2	2	2	2	2	2	2	2	2
S	50	299	117	668	238	90	829	170	149	81	116	118	185	728	124	129	120	108
Sb	0.5	<0.5	<0.05	<0.5	<0.5	<0.5	<0.5	<0.5	0.6	<0.5	<0.5	<0.5	<0.05	<0.05	<0.05	<0.5	<0.5	<0.5
Sc	0.5	7	3.7	2.6	3	3.5	3.6	8.2	9.5	7	4.7	2	4.1	3.5	3.6	6.2	5	2.2
Sm	0.02	<0.02	<0.02	<0.02	<0.02	<0.02	<0.02	0.63	1.97	<0.02	<0.02	<0.02	<0.02	<0.02	<0.02	<0.02	<0.02	<0.02
Sn	0.1	0.3	0.3	0.3	0.3	0.3	0.4	0.6	1.1	0.3	0.4	0.3	0.3	0.3	0.4	0.3	0.4	0.3
Sr	1	3.3	52.3	<1	108.7	16.6	22.3	185	171.6	5.4	63	35.7	41.3	119	345.5	126	363.5	59.3
Ta	0.1	0.25	0.2	0.23	0.29	0.29	0.24	0.4	0.56	0.17	0.24	0.29	0.26	0.24	0.33	0.26	0.28	0.25
Tb	0.1	0.12	0.12	0.12	0.12	0.12	0.12	0.26	0.44	0.14	0.12	0.12	0.12	0.13	0.17	0.14	0.14	0.12
Th	0.1	<0.1	<0.1	<0.1	<0.1	<0.1	<0.1	<0.1	0.44	<0.1	<0.1	<0.1	<0.1	<0.1	<0.1	<0.1	<0.1	<0.1
TI	0.1	<0.1	<0.1	<0.1	<0.1	<0.1	<0.1	<0.1	<0.1	<0.1	<0.1	<0.1	<0.1	<0.1	<0.1	<0.1	<0.1	<0.1
Tm	0.1	<0.1	<0.1	<0.1	<0.1	<0.1	<0.1	<0.1	0.14	<0.1	<0.1	<0.1	<0.1	<0.1	<0.1	<0.1	<0.1	<0.1
U	0.1	<0.1	0.1	<0.1	1.6	<0.1	<0.1	0.2	0.6	0.3	0.1	0.1	1.7	0.7	0.2	0.3	0.3	0.1
V	1	25	33	13	22	22	29	51	80	46	17	10	17	20	19	29	26	12
Y	0.5	<0.5	<0.5	<0.5	<0.5	<0.5	<0.5	4.9	12.7	1.5	<0.5	<0.5	<0.5	0.5	1.7	1.1	1.7	<0.5
Yb	0.05	0.3	0.3	0.3	0.3	0.4	0.4	0.7	1.2	0.8	0.2	0.2	0.2	0.3	0.3	0.4	0.4	0.2
Zn	1	45	41	52	39	57	63	49	63	96	31	27	25	31	25	57	38	26
Zr	5	<5	<5	<5	<5	<5	<5	27	44	<5	<5	<5	<5	<5	5	<5	<5	<5

Table 3: Continuing …

Sample		**R-04**	**R-02**	**R-22**	**R-24**	**R-38**	**R-42**	**R-43**	**R-45**	**R-47**	**R-48**	**R-49**	**R-50**	**R-51**	**R-53**	**R-56**	**R-58**	**R-41**
Lith.a		**TZ**	**FCO**	**FCO**	**FCO**	**FCO**	**FCO**	**FCO**	**FCO**	**FCO**	**FCO**	**FCO**	**FCO**	**FCO**	**FCO**	**FCO**	**FCO**	**SstO**
wt.%	DL																	
Al_2O_3	0.05	6.96	6.45	2.47	5.56	6.68	6.22	4.57	8.62	9.68	6.23	8.26	7.62	15.5	8.15	7.65	8.89	9.42
CaO	0.05	1.82	1.36	0.38	1.12	0.28	15.06	0.35	0.67	0.23	0.21	1.77	1.46	0.88	0.27	0.19	0.48	0.22
Fe_2O_3	0.05	12.73	8.9	6.49	9.36	12.7	6.95	42.55	13.04	12.8	14	14.5	8.71	14.5	22.3	22.19	10.4	27.73
K2O	0.05	1	0.64	0.28	1.2	1.51	0.35	0.75	1.93	3.09	2.4	2.76	1.51	3	3.04	2.89	2.59	2.95
MgO	0.05	4.19	7.5	1.93	3.54	2.66	6.86	2.2	4	3.17	1.58	2.72	3.42	5.68	2.53	2.58	3.77	3.27
MnO	0.05	0.15	0.12	0.07	0.1	0.15	0.14	0.22	0.24	0.11	0.08	0.07	0.26	0.21	0.14	0.21	0.15	0.2
Na_2O	0.05	1.42	1.57	0.39	0.76	1.26	0.58	<	1.52	0.72	<	0.15	1.32	3.05	<	<	0.93	<
P_2O_5	0.05	0.13	0.13	<	0.15	<	0.14	0.07	0.11	0.05	0.08	<	0.13	0.49	0.12	0.06	0.1	<
SiO_2	0.05	66.07	67.1	86.1	74.2	71	44.95	43.35	64.54	65.31	72.1	63.9	7.5	49	58.8	59.06	68	48.93
TiO_2	0.05	0.87	0.94	0.14	0.52	0.71	0.67	0.13	1.23	0.99	0.46	0.81	0.83	2.91	0.55	0.55	0.92	0.72
LOI	0.05	4.12	4.76	1.49	3.05	2.24	17.34	2.11	3.36	3.15	2.09	4.43	3.71	4.48	2.74	2.82	3.35	3.61
Total		99.46	99.5	99.7	99.6	99.7	99.94	99.54	99.26	99.3	99.3	99.3	36.47	99.6	99.7	99.54	99.5	99.25
mg/kg	DL																	
As	0.1	0.4	2.5	4.4	4.1	2.4	8.3	12	2.8	3.3	5.3	1.6	3.5	<0.1	6.9	7.2	3.8	38.3
Ba	1	85	63	32	74	122	186	46	131	96	104	82	116	270	193	235	89	86
Be	0.2	0.5	0.4	<0.2	0.8	0.6	1.6	1.3	1	1.2	0.7	1.1	0.9	1.1	1.1	0.9	1.2	0.6
Ce	0.5	22	19	3	19	29	25	<1	30	41	19	27	27	16	25	21	29	17
Co	1	12014	128	60.3	65.7	163	328.3	284.9	110.1	133.7	106	101	78.6	122	132	216.3	85.6	47.2
Cr	1	2195	1757	1301	1790	3254	>1%	>1%	2558	2582	3026	2508	1593	293	7162	8495	1882	3373
Cs	0.5	1.7	1.1	1.2	2.6	0.9	1.2	3.2	3.2	5.9	4	7.1	2.7	2.3	5.2	4.3	5	5
Cu	1	34	23	39	23	29	22	36	23	23	145	53	27	6	82	34	17	14
Dy	0.02	2.45	1.99	0.64	2.29	2.19	2.57	1.55	2.98	2.49	1.9	2.08	2.84	3.32	2.83	2.06	2.87	2.07
Er	0.05	1.14	1.08	0.41	1.24	1.22	1.47	1.01	1.39	1.44	1.21	1.25	1.67	1.68	1.55	1.29	1.61	1.34
Eu	0.1	0.9	0.7	0.14	0.71	0.81	0.72	0.38	1.07	0.82	0.54	0.67	0.92	1.09	0.87	0.56	0.93	0.62
Gd	0.05	2.97	2.24	0.33	2.32	2.34	2.39	1.12	3.31	2.7	1.87	2.02	3.09	3.32	2.73	2.04	2.83	1.96
Hf	0.5	<0.5	0.67	<0.5	<0.5	0.77	0.75	<0.5	1.12	1.38	<0.5	1.18	1.18	<0.5	0.9	0.63	1.34	0.6
La	1	12	10	2	11	17	15	2	16	14	10	14	17	9	14	11	14	9
Li	1	13	15	6	13	13	10	7	21	11	<1	6	14	32	4	2	14	36
Lu	0.1	0.11	0.12	<0.1	0.14	0.14	0.14	0.12	0.15	0.17	0.11	0.14	0.2	0.13	0.19	0.15	0.16	0.15
Mo	0.1	21	20	16	17	18	11	12	7	11	17	11	13	<0.1	21	12	11	2
Nb	1	3.6	4.1	<1	3.4	5.3	4.9	1.4	3.4	5.8	3.4	6	5.7	5	4.8	4.3	5.8	4
Nd	0.5	13.5	10.2	1	10.2	15.5	12	4.5	16.2	13	9.1	12.6	14.8	12.7	13.6	10.8	13.2	8.4
Ni	1	1741	2167	858	1100	2894	5816	4223	2277	2535	2141	2499	1247	1870	3179	3959	1585	507
P	10	568	553	95	643	132	198	423	474	233	287	132	521	1518	469	277	392	483
Pb	1	3	<1	<1	3	5	11	7	<1	<1	5	3	<1	<1	7	6	<1	<1
Pr	0.05	3.02	2.31	0.3	2.32	3.59	2.99	0.8	3.64	3.09	2.35	2.98	3.43	2.42	3.16	2.34	3.04	1.83
Rb	1	22	18	9	29	40	92	25	48	88	71	83	41	61	82	76	67	8
S	50	129	149	132	120	111	119	112	121	120	122	117	116	73	113	114	115	314
Sb	0.5	<0.5	<0.5	0.8	<0.5	0.5	1.8	3.5	<0.5	0.7	0.9	0.8	0.7	<0.5	2.7	2.3	0.8	1.5

Sc	0.5	13.2	10.9	4	11.1	13.7	25.8	30.9	18.5	18.2	13.9	14.8	13.7	15.3	21.7	20.7	15.1	9.5
Sm	0.02	2.76	2.07	0.17	2.14	2.71	2.23	0.83	3.3	2.63	1.77	2.06	2.94	2.91	2.69	1.93	2.68	1.73
Sn	0.1	0.9	1	0.7	0.8	0.9	1.1	0.6	0.9	1	1	1	1.2	0.7	1	1	1.1	0.7
Sr	1	97	88.6	15.2	12.3	83.2	40.5	30	102.9	50.6	25.3	22.5	103.9	110	55.6	47.7	53.9	374.2
Ta	0.1	0.4	0.55	0.35	0.56	0.7	0.77	0.41	0.5	21.68	0.62	0.83	0.77	0.51	0.73	0.68	0.76	0.57
Tb	0.1	0.53	0.41	0.21	0.46	0.46	0.49	0.35	0.61	0.54	0.45	0.46	0.61	0.63	0.55	0.44	0.53	0.43
Th	0.1	0.53	0.45	0.27	0.66	0.99	2.04	<0.1	0.93	1.94	1.44	1.87	1.76	0.51	2	1.73	1.89	0.54
TI	0.1	<0.1	<0.1	<0.1	<0.1	<0.1	0.37	<0.1	0.13	0.22	0.25	0.39	0.11	0.14	0.34	0.32	0.22	0.11
Tm	0.1	0.13	0.12	<0.1	0.15	0.13	0.14	0.11	0.15	0.14	0.11	0.16	0.19	0.18	0.18	0.13	0.17	0.16
U	0.1	0.6	0.4	0.3	0.6	0.7	0.9	0.5	0.7	0.8	0.8	0.8	1	0.5	0.9	0.7	0.7	1.3
V	1	129	77	74	108	112	231	385	98	114	125	131	129	62	236	178	96	128
Y	0.5	11.8	10.4	3.7	13.1	10.9	14	11.7	13.3	13.2	8.4	10.9	17	16.4	14.5	11.5	14.8	11.9
Yb	0.05	1.4	1.1	0.6	1.4	1.6	3	4	1.5	1.8	1.6	1.9	1.8	1.5	2.7	2.4	1.6	1.4
Zn	1	89	85	46	85	103	247	292	116	121	74	100	93	145	164	177	87	67
Zr	5	27	46	15	42	56	43	20	45	83	23	62	60	20	53	47	72	45

5. Discussion

Olistostromes, as stated in this work, are slow-moving sliding bodies that normally are not likely to be very large in the sedimentary basins. Nevertheless, some bodies are 200–300 m thick and cover hundreds of square kilometers of areas. Moreover, the base of MTC is always lens-shaped, with erosional surfaces and scars [2, 36], indicating subsurface erosion cohesive debris flows incompatible with viscous laminar flow. Many kinds of MTD, including olistostromes, occur in the epi-sutural/wedge-top basin succession [7, 8, 36-47].

Several authors have discussed the processes and differences in the formation of Mélanges and olistostromes [5, 7, 49, 50]. Olistostromes and mass-transport deposits are predominantly gravitational and widespread in subduction-accretion complexes and orogenic belts. The tectonic conditions where different olistostromes originate are linked [7, 51]). Researchers can assess the role of olistostromal occurrences in the evolution of ancient orogenic belts and exhumed subduction complexes thanks to their preservation in the geological record and study of their internal structure. Olistostromes are indicators of regional tectonic events if their emplacement is widespread. The stacking, slumping, debris flows, blocky flows and turbidity currents generate olistostromes' complex stratigraphic relationships [44, 52, 53].

In petrographic examinations of sedimentary rocks, the provenance area concept is used to characterize the source region and transport direction of the sedimentary rock components. Thus, the components decomposed and eroded are carried from the source area, and are deposited in any basin, providing crucial information about the source region [63, 65]. In the Choman-Rayat area, the olistostromes lithotypes outcrops are widely spread. The field work, and the mineralogical, petrographic, and geochemical data, indicate that the serpentinites as well as carbonate rocks of the Walash Group serve as the bedrock and wall rock of the investigated olistostromes. The Walash Group has previously been described as a back-arc, calc-alkaline, and alkaline suite of rocks originated during the Eocene age [54]. The majority of the clasts that come from sandstones are fossils and pieces of fossils. Algae, found in fossils, shows the environments on the shelf and slope in the northern part of the study area [66]. On the top portions of sandstone olistostrome lithotype, which represent a series of layered sandstones above the "conglomerate sequence" and display a high degree of internal deformation, rock pieces are discovered. They have a homogenous petrography (with clay and sandstones predominating), yet they exhibit evidence of gravity transfer. Such accumulations with significant internal deformations have been regarded as slump deposits [67, 68].

A comparative example is the Iranian Late Miocene Makran olistostrome deposits. The Makran olistostrome is intercalated within the sedimentary sequence of the tectonic wedge [55]. The Makran olistostrome does not overlie an undisturbed succession, but a previously folded and eroded substratum of variable ages. The olistostrome and its substratum have been later folded and thrusted. Hence, similar reasoning may be applied to the Rayat olistostrome, whose structural and textural characteristics demonstrate that it is created by the southerly (trench-ward) migration of a fluid into a viscoelastic underwater mass flow. The lithoclasts of the Rayat olistostromes are often sub-angular to rounded in shape, larger than other lithotype lithoclasts. There is evidence in the field that the smallest clasts with different sizes, from grains to centimeters, are sedimentary, occurring as rounded in sandy matrix in very poorly sorted mass flow.

Late Miocene and Pliocene sedimentation in the area shows an upward coarsening of terrigenous molasse succession [56]. Eocene/Oligocene Miocene Red Beds are covered, while the Mawat ophiolite-bearing nappe is forced over the earlier (Late Miocene) Walash-Naopurdan magmatic arc nappe, serpentinite has already been deposited on the Arabian margin [27]. This contradicts the thrust zone reported in another part of the Zagros Suture Zone that happened out of sequence in the southwest Zagros Suture Zone [57].

Frequently, the contact between serpentinites and ophicarbonates and a metasomatic horizon is unclear and inconsistent in the Rayat area. In this horizon, rocks usually have important carbonate mineral layers interspersed with other mineral layers. This metasomatic horizon is characterized by the foliation indicated by these gray layers. The bottom portion of the exposed olistostromes bodies consists of bodies of fine-grained serpentinite matrix olistostromes (SO) lithotype. The OpCO lithotype contacts the OS lithotype. It is yellowish-green in color. Due to crushing and movement of serpentinites, mm- to cm-sized clasts float within carbonate minerals [51]. The ferruginous serpentinite olistostromes (FSO) and ferruginous ophiocarbonatic olistostromes (FOpCO) lithotypes are re-cemented by iron oxide, such as hematite. Following successful serpentinization by hydrothermal activity, serpentinite peridotite may eventually be transformed by a tectonic process into various rock lithotypes. Olistostromes lithotypes are occurred, faulted, subduction faulted cracked porous zone of ultramafic rocks, acting as a pathway for moving fluids.

The Rayat area's serpentinites, which are discrete masses that reflect serpentinized for-arc mantle wedge peridotites, are deposited during diapiric upwelling into a non-accretionary for-arc tectonic environment during the Paleocene to Eocene age [73]. Fluids from the mantle wedge slab lead to the serpentinization of the peridotites. Subducted material may undergo dehydration reactions, sediment pore water ejection, porosity decrease, slab-derived fluids rising to the surface, and ultimately serpentinization occurring of upper mantle rocks in for-arc [73].

The mineralogical, petrographic, and geochemical information may be used to derive the following general properties of the investigated lithotypes. The Walash Group's serpentinites, which have earlier been described as a back-arc, calc-alkaline, and alkaline suite of rocks developed during the Eocene age, serve as both the bedrock and the wall rock of the mineralization under study [27, 54]. However, with the information from this study, namely the peridotites and their comparable serpentinites, there is a greater proof that the serpentinites are the parent rock of the detected mineralization. The investigated Cr-spinels have a variety of forms, ranging from rounded to angular, but often lack a euhedral form.

According to the results, SiO_2, CaO, and K_2O are introduced to quartz and carbonate-veins. P_2O_5 is incorporated into the structure of carbonate minerals. The main phases that contain Fe are hematite, magnetite, and spinel, but other minerals, such as clay minerals and serpentines, also contain this element. Nickel is present in the structure of different minerals such as serpentines and hematite, but the highest amount of it is in the structure of chlorite. Cobalt is mainly associated with phases such as magnetite, hematite and chlorite.

The rare earth elements in almost all of the investigated lithologies are quite similar, decreasing and exhibiting a metasomatized mantle-like composition [34, 35]. In the majority of samples, rare earth element concentrations are fairly low.

The recovered microfossils suggest shallow-water subtidal assemblages from an inner-platform environment, possibly a shelf lagoon with open circulation decimetric to metric Paleocene-Eocene olistostrome lithotype. Beds have poor sorting, with decimetric pieces and metric blocks. This sequence has clasts, matrix-supported. In contrast to clay and marl clasts, olistoliths are composed of sandstones, basic volcanic rocks, conglomerates, and lithoclasts. Dasycladalean algae (primarily Salpingoporella muelhbergii and Falsolikanella danilovae), benthic foraminifera, and peloids/micritic pellets are the most notable characteristics of bio-peloidal grainstone [69, 72]. In sandstone olistostromes lithotypes, mostly various types of foraminifera and algae are observed, those fossils are replaced by quartz and calcite.

Carbonate lithoclast in SstO shows abundant intact microfossils of green alga dasyclads neomeris, trinocladus perplexus elliott, sponges' fragments, corals and forams (miliolid, and nummulites, opercoulina ammonida). These daysclad algae are typical of the Paleocene-Eocene period in Kurdistan, pertaining probably to the Sinjar Fm equivalent. The bioclasts are significant indicators of the dating and formation age of the olistostromes in the Choman area, hence paleotectonic interpretation. The minerals fragments are including quartz grains, feldspar and pyrite spots.

Hydrothermal activities are evident in the area. Evidences of hydrothermal activities include serpentinization, and listvenitization [25] in nearby serpentinites. The presence of quartz veins and ferruginous olistostromes lithotypes is another evidence for hydrothermal fluids activities. The high amount of elements such as Fe, Ni, and Co could be related to hydrothermal activities and leaching them from other rocks. Hydrothermal influence on the area is one of the factors that created different types of olistostrome lithotypes, such as ferruginous one.

Nano-size crystal mineralization in fresh water and marine environment is predominantly represented by Fe and Si, implying hydrothermal mobility and precipitation. Literature shows that bacteria-iron interactions may cause iron precipitation and deposits [30, 32]. The overall interaction implies dissolved Fe (II) oxidation by cyanobacterially-produced O2 and/or chemolithotrophic bacteria [33] (Fig. 15).

The mineralization chemistry that is made of nano-size crystals is mainly represented by Fe and Si, suggesting elements mobility and precipitation during a hydrothermal event. The bacteria-iron interactions that can produce iron precipitation and deposits are well known in literature [30, 32].

5.2 Conceptual Model

The olistostromes lithotypes in Rayat area present a complex case study. Although at this stage a complete genetical model is not possible due to the lack of significant background geological structural information of the area, an interpretation of the various mechanisms that lead to the formation of the observed olistostromes outcrops can be expanded.

The particular time of development of the body is identified; however, the overall geological history of the area would imply a Paleocene-Eocene epoch [73, 74]. Nevertheless, a conceptual model of formation is described, with continued development to build a more complete genetic model (Fig. 16).

The first step includes the sub-seafloor or seafloor exhumation of Walash Group bedrock peridotites, resulting in seawater circulation, hydration and strong serpentinization. The development of the serpentinization olistostromes mechanism owing to saltwater contact with peridotites would have increased their porosity and therefore volume [75], causing near seafloor structural fracturing, faulting, and slope failure. This structural failure within the marine environment creates serpentinite olistostromes (see Fig. 16a) of serpentinite containing material [76] (Fig. 16a). The olistostromes serpentinite is deposited in deeper areas near the serpentinites, which are concurrently affected by the hydrothermal alteration ophiocarbonatic olistostrome lithotype deposited and venting enriched in Ca-Ni exhalates (Fig. 16b).

The hydrothermal fluids that influenced the sub-seafloor porous serpentinites accelerate the development of magnetite (from spinel and primary minerals) as alteration products while also depositing Ni- and calcite inside the rich matrix (Fig. 16b). The top half exhibits a brecciated structure due to a chaotic mixing of serpentinite lithoclasts, hydrothermally formed Fe and increasing minerals like quartz, and other exhalative-originated Fe-Si-rich phases (Fig. 16c).

In the second step, under oxidizing circumstances, the minerals in the higher sections of the system are transformed into oxides (Fig. 16d). Moreover, the produced bed ferruginous olistostromes lithotype provides the present bedding structure on the upper strata. As the hydrothermal impact slowed, both in terms of temperature and venting activity, a more oxidative environment develops, resulting in the complete oxidation, Fe and Si (Fig. 16e) [83]. A transition zone has been formed at the interface between the OpCO and FCO beds, reflecting the front of oxidation, which progresses as the strata are revealed.

The effect of the hydrothermal system is eliminated in the third stage, when the whole system is exposed to lateral displacement, and the depositional conditions become less turbiditic and detrital (Fig. 16e) [77]. The examined series is covered at the top by sedimentary deposition of ferruginous conglomerate olistostromes (FCO) and sandstone olistostromes (SstO) lithotypes interbedded with claystones (Fig. 16f).

Eventually, the serpentinite along bodies package as a whole has been implicated in the ophiolitic nappe obduction by actually representing the latter's ophiolitic m'elange [74]. The occurrence inside ultramafic–mafic terrain is uncommon and can only be explained as part of the ophiolitic mélange, most likely formed in the Arabian plate during the Paleocene–Eocene period and integrated inside the thrust activity along the ductile-tobrittle deformation of the enclosed volcanic rocks. However, the presence of olistostromes is important in understanding the thermotectonic development of the examined region. The temperature of the hydrothermal impact has effects on the rock type absorption [81].

5.2 Implications for Regional Exploration

A complete lithological geochemical and tectonic mapping of this part of the country has not yet been completed. Previously, some papers were published about mineralization of the area. The main reported mineralization of the area included chromite, iron, nickel and cobalt. Chromite mineralization occurred in ultramafic and their equivalent serpentinites. The chromites were of podiform types with high concentration of chromium (>40 %) [17, 18]. Iron, nickel and cobalt occurred in gossanite like deposits [19]. Moreover, according to [25], the area was affected by several stages of hydrothermal activities and these activities led to the formation of listvenites, which represent a good source of metals, such as Au and Ag. In addition, there is a significant potential for the extraction of other metals in this area, such as platinum group elements (PGEs), due to the presence of chromitites. From the geological point of view, vast majority of Rayat is composed of ophiolitic mélange, and multi lithotypes of olistostromes present significant challenges when attempting to identify and characterize potential mineralization zones.

The geochemical record of the examined lithotype olistostromes reveals an abundance pattern for several metals, such as iron, nickel, chromium, and cobalt; these elements are in quite high concentrations. Finally, it can be concluded that introducing olistostromes with high potential of mineralization can be a good guide for companies for the investment in the Rayat area for mineral exploration.

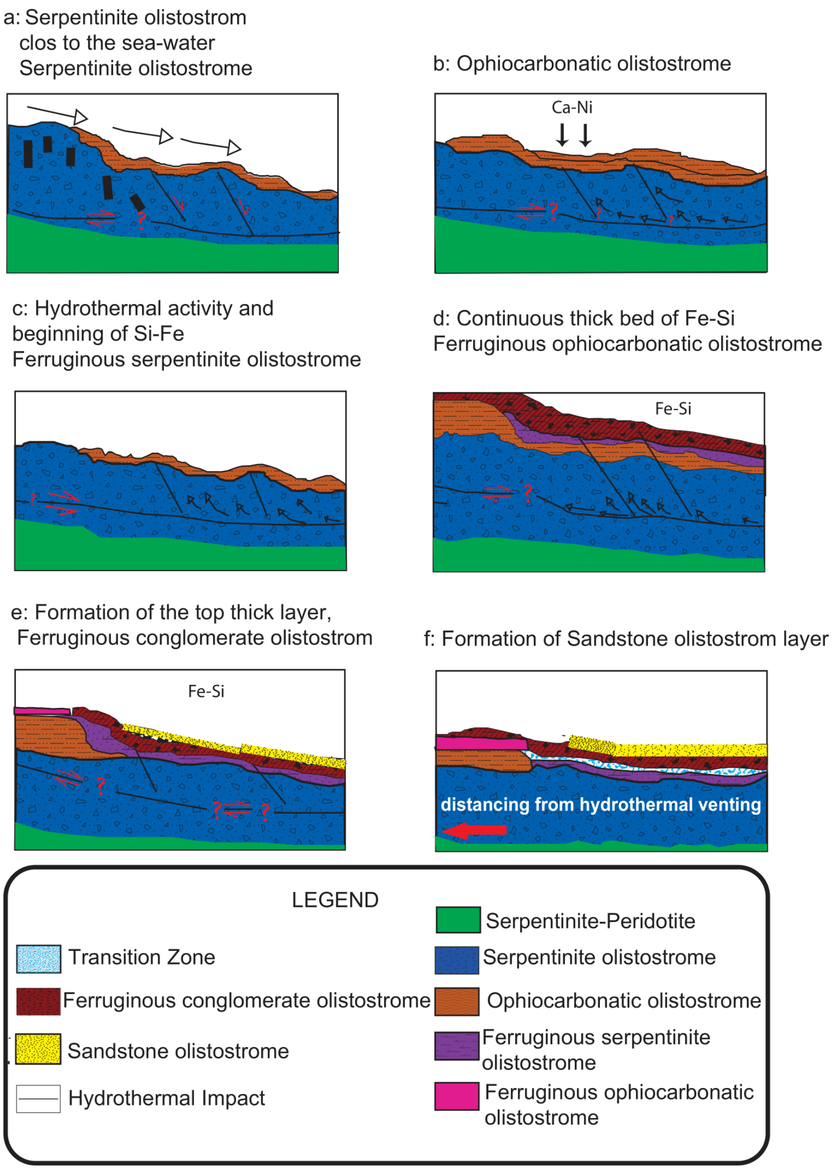

Fig. 16: Diagram (not in scale) model of the Rayat olistostrome lithotype and development in the marine environment, but not considering the post-forming tectonic deformation and uplift of the Walash Ophiolite mélange

6. Conclusions

The multi olistostromes lithotypes of Choman- Rayat area in the NE Iraqi Kurdistan region are described here for the first time. This study shows that the different types of olistostrome lithotypes and their characteristic features are closely related to the specific tectonic settings of their formation. Our recent fieldwork study in the previously restricted Choman-Rayat area in NE Iraqi Kurdistan in terms of accessibility reveals an assemblage of olistostromes lithotypes with various lithological and geochemical characteristics comprising of SO, OpCO, FSO, FOpCO, FCO and SstO. The parent rocks of those olistostromes lithotypes are considered the serpentinites, clasts, carbonates and sandstones of the Walash-Naopurdan Group. The discovery of these olistostromes lithotypes in the Rayat region, with their numerous lithologies and geochemistry contributes significantly to the geology of Kurdistan and the potentiality of highlighting new economic mineralization-rich areas. Moreover, the findings provide the basis for an updated knowledge about lithotypes-based olistostromes, aiming at improving the Rayat region of Iraq's Kurdistan Region's ability to manage its natural resources.

This study shows a significant relationship between the different kinds of olistostrome lithotypes, their distinctive traits, and the varied tectonic conditions in which they arose. The mineral association and geochemical variation among them reflect seven different lithotypes of olistostromes occurrence including SO, OpCO, FSO, FOpCO, FSO, FCO, and SstO. Ferruginous conglomerate olistostromes show a high concentration of Fe_2O_3, associated mainly with quartz and a variety of minerals. According to the geochemical results, ferruginous conglomerate olistostromes (FCO) lithotype is rich in SiO2 (43.35-7423 wt.%), while it has the highest amount of Fe_2O_3, which is 42.55 wt.%. FCO has the greatest amount of Nickel and Cr (5,816 mg/kg and 8,495 mg/kg, respectively). SstO (507 mg/kg) has the lowest concentration of Nickel. In contrast, Cobalt shows a rise in concentration from the top horizon of FCO represented by 328 mg/kg. The studied samples reflect the different types of olistostromes lithotypes. Ni, Co, and Cr are highly enriched elements in the Fe-rich mineralized zone. Petrological studies indicate that the sandstone olistostromes lithotype (SstO) samples are quartz and calcite, sometimes fossiliferous (the main constituents are foraminifera and algae). The samples are generally pure sandstone, as shown by the petrographical analysis of thin sections. Many types of fossils have been identified. The SEM-EDS results indicate an increase in concentrations of CaO in FOpCO, SstO and calcite mineral, and a decrease in the concentrations of K_2O, and Cr_2O_3, showing the enrichment of Fe_2O_3 concentration in FOpCO, and FCO lithotypes in the hematite and magnetite mineral. Whereas SstO shows high amount of SiO_2 in quartz.

Under this environment, bacterial morphs play an important role, as indicated by the presence of abundant bacteria embedded within the matrix of the studied rock samples, in relation to both the formation of the different minerals as well as in their syn-or epigenetic oxidation.

Acknowledgments

The authors would like to thank scientific research members for their help and support during this research.

References

[1] Abbate, E.; Bortolotti, V. and Passerini, P. (1970). Olistostromes and olistoliths. *Sedimentary Geology*, 4(3-4):521-557.

[2] Pini, G.A. Camerlenghi, A. Festa, A. Lucente, C.C. Codegone, G. (2012). Sedimentary mélanges and fossil mass-transport complexes: a key for better understanding submarine mass movements? in Submarine mass movements and their consequences. *Springer*:585-594.

[3] Andronache, A. Pleş, G. Bucur, I. Ilieş, Iulia A. (2022). Microfacies and age of the Ceahlău Massif carbonate olistoliths (Eastern Carpathians, Romania): Remnants of a lowermost Cretaceous carbonate platform. *Proceedings of the Geologists' Association*.

[4] Bates, R.L. and Jackson, J.A. (1987). Glossary of geology: American geological institute. *Alexandria, Virginia*:788.

[5] Hsü, K.J. (1968). Principles of mélanges and their bearing on the Franciscan-Knoxville paradox. *Geological Society of America Bulletin*, 79(8):1063-1074.

[6] Raymond, L.A. (1984). Melanges: their nature, origin, and significance. *Geological Society of America Special Paper*, 198:7-20.

[7] Festa, A. Pini, G.A. Dilek, Y. Codegone, G. (2010). Mélanges and mélange-forming processes: a historical overview and new concepts. *International Geology Review*, 52(10-12):1040-1105.

[8] Festa, A. Pini, G.A. Dilek, Y. Codegone, G. Vezzani, L. Ghisetti, F. Lucente, C.C. Ogata, K. (2010). Peri-Adriatic mélanges and their evolution in the Tethyan realm. *International Geology Review*, 52(4-6):369-403.

[9] Festa, A. Dilek, Y. Gawlick, H.J. Missoni, S. (2014). Mass-transport deposits, olistostromes and soft-sediment deformation in modern and ancient continental margins, and associated natural hazards, *Marine Geology*: p.1-4.

[10] Festa, A. Ogata, K. Pini, G.A. Dilek, Y. Alonso, J. (2016). Origin and Significance of Olistostromes in the Evolution of Orogenic Belts: *A Global Synthesis. Gondwana Research*, 39:180-203.

[11] Faghih, A.; Kusky, T. and Samani, B. (2012). Kinematic analysis of deformed structures in a tectonic mélange: a key unit for the manifestation of transpression along the Zagros Suture Zone, Iran. *Geological Magazine*, 149(6):1107-1117.

[12] Rast, N. and Horton Jr. J. W. (1989). Melanges and olistostromes in the Appalachians of the United States and mainland Canada; An assessment. *Geological Society of America Special Paper*, 228:1-16.

[13] Jassim, S.Z. and Goff, J.C. (2006). Geology of Iraq: Dolin. *Geological Society of London*, 5pp.

[14] Fouad, S.F. (2012). Western Zagros fold–thrust belt, part I: The low folded zone. *Iraqi Bulletin of Geology and Mining*, 5:39-62.

[15] Al-Bassam, K.S. (2013). Mineral resources of Kurdistan region, Iraq. Iraqi Bulletin of Geology and Mining, 9(3):103-127.

[16] Buda, G. and Al-Hashimi, W. (1977). Petrology of Mawat ophiolitic complex. *Jour. Geol. Soc. Iraq*, X: p. 69-98.

[17] Ismail, S.A. Arai, S. Ahmed, A.H. Shimizu, Y. (2009). Chromitite and peridotite from Rayat, northeastern Iraq, as fragments of a Tethyan ophiolite. *Island Arc*, 18(1):175-183.

[18] Ahmed, I.N.; Kettanah, Y.A. and Ismail, S.A. (2020). Genesis and tectonic setting of high-Cr podiform chromitites of the Rayat ophiolite in the Zagros Suture Zone, northeastern Iraq. *Ore Geology Reviews*, 123:103583.

[19] Pirouei, M. Kolo, K. Kalaitzidis, S. Abdullah, S.M. (2021). Newly discovered gossanite-like and sulfide ore bodies associated with microbial activity in the Zagros ophiolites from the Rayat area of N.E. Iraq. *Ore Geology Reviews*, 135:104191.

[20] Watkinson, Hak, J.D. and Al-Bassam, K. (1983). The origin of the Marabasta base metal deposit, NE Iraq. *Věstník Ústředního ústavu geologického*, 58(3):141-148.

[21] Numan, N.M. (1997). A plate tectonic scenario for the Phanerozoic succession in Iraq. *Iraqi Geological Journal*, 30(2): 85-110.

[22] Lawa, F. Koyi, H. and Ibrahim, A. (2013). Tectono-stratigraphic evolution of the N.W. segment OF the Zagros fold-thrust belt, Kurdistan, NE Iraq. *Journal of Petroleum Geology*, 36(1):75-96.

[23] Vasiliev, M. and Pentelkov, V. (1962). Prospecting exploration of the Bardi-Zard chromite occurrence and adjacent areas. *Iraqi Geological Survey*.

[24] Pirouei, M. Kolo, K. and Kalaitzidis, S.P. (2020). Chromium-rich muscovite mineralization in Zagros ophiolites in Iraqi Kurdistan: a study on fuchsite paragenetic association with listvenite types. *Arabian Journal of Geosciences*, 13(17):1-13.

[25] Pirouei, M. Kolo, K. and Kalaitzidis, S.P. (2020). Hydrothermal listvenitization and associated mineralizations in Zagros Ophiolites: Implications for mineral exploration in Iraqi Kurdistan. *Journal of Geochemical Exploration*, 208:106404.

[26] Al-Mehaidi, H. (1974). Report on Geological investigation of Mawat-Chromite area Iraq. *Iraqi Geological Survey*.

[27] Ali, S.A. Buckman, S. Aswad, K.J. Jones, B.G. Ismail, S.A. Nutman, A.P. (2013). The tectonic evolution of a Neo-Tethyan (Eocene–Oligocene) island-arc (Walash and Naopurdan groups) in the Kurdistan region of the Northeast Iraqi Zagros Suture Zone. *Island Arc*, 22(1):104-125.

[28] Moores, E.M. Kellogg, L.H. and Dilek, Y. (2000). Tethyan ophiolites, mantle convection, and tectonic" historical contingency": A resolution of the" ophiolite conundrum". *Special papers Geological society of America*: p. 3-12.

[29] Sissakian, V.K. and Fouad, S.F. (2015). Geological map of Iraq, scale 1: 1000 000, 2012. *Iraqi Bulletin of Geology and Mining*, 11(1): 9-16.

[30] Konhauser, K.O. (1998). Diversity of bacterial iron mineralization. *Earth-Science Reviews*, 43(3-4):91-121.

[31] Kolo, K. Konhauser, K. Krumbein, W.E. Ingelgem, Y.V. Hubin, A. Claeys, P. (2009). Microbial dissolution of Hematite and associated cellular fossilization by reduced iron phases: a study of ancient microbe-mineral surface interactions. *Astrobiology*, 9(8): 777-796.

[32] Konhauser, K.O. Robbins, L.J Pecoits, E. Peacock, C. Kappler, A. Lalonde, S.V. (2015). The Archean nickel famine revisited. *Astrobiology*, 15(10):804-815.

[33] Peacock, C.L. Lalonde, S.V. and Konhauser, K.O. (2016). Iron minerals as archives of Earth's redox and biogeochemical evolution. *EMU notes in Mineralogy*, 17:113-164.

[34] Zhou, M.F.; et al. (2004). Geochemistry and petrogenesis of 270 Ma Ni–Cu–(PGE) sulfide-bearing mafic intrusions in the Huangshan district, Eastern Xinjiang, Northwest China: implications for the tectonic evolution of the Central Asian orogenic belt. *Chemical Geology*, 209(3-4):233-257.

[35] Tsikouras, B. Karipi, S. Grammatikopoulos, T.A. Hatzipanagiotou, K. (2006). Listwaenite evolution in the ophiolite melange of It Mountain (continental Central Greece). *European Journal of Mineralogy*, 18(2):243-255.

[36] Pini, G.A. (1999). Tectonosomes and olistostromes in the Argille Scagliose of the Northern Apennines, Italy. *Geological Society of America*: p. 73.

[37] Bettelli, G. Bonazzi, U. Fazzini, P. Gasperi, G. Gelmini, R. Panini, F. (1989). Nota illustrativa alla Carta Geologica Schematica dell'Appennino modenese e delle aree limitrofe. *Memorie Della Società Geologica Italiana*, 39:487-498.

[38] Mutti, E. Papani, L. Di Biase, D. Davoli, G. Mora, S. Segadelli, S. Tinterri, R. (1995). Il Bacino Terziario Epimesoalpino e le sue implicazioni sui rapporti tra Alpi ed Appennino. *Memorie di Scienze Geologiche*, 47:217-244.

[39] Martelli, L. Cibin, U. Di G.A Catanzariti, R. (1998). Litostratigrafia della Formazione di Ranzano (Priaboniano-Rupeliano, Appennino Settentrionale e Bacino Terziario Piemontese). *Bollettino della Società geologica italiana*, 117(1):151-185.

[40] Panini, F. Fioroni, C. Fregni, P. Bonacci, M. (2002). Le rocce caotiche dell'Oltrepo Pavese: Note illustrative della Carta Geologica dell'Appennino vogherese tra Borgo Priolo eRuino. *Atti Ticinenesi Di Scienze Della Terra*, 43:83-109.

[41] Filippo, P.; Chiara, F. and Paola, F. (2013). Le Brecce argillose di Musigliano (Appennino Vogherese – Tortonese): *Dati stratigrafici preliminari Rendiconti Online Della Società Geologica Italiana*, 26:21–31.

[42] Pini, G. (2004). The role of olistostromes and argille scagliose in the structural evolution of the Northern Apennines. *Memorie Descrittive della Carta Geologica d'Italia, 63:1-14.*

[43] Festa, A. (2011). Melanges: Processes of formation and societal significance. *Geological Society of America Special Paper*, 480:215-232.

[44] Festa, A. and Codegone, G. (2013). Geological map of the External Ligurian Units in western Monferrato (Tertiary Piedmont Basin, N.W. Italy). *Journal of Maps*, 9(1):84-97.

[45] Remitti, F. Vannucchi, P. Bettelli, G. Fantoni, L. Panini, F. Vescovi, P. (2011). Tectonic and sedimentary evolution of the frontal part of an ancient subduction complex at the transition from accretion to erosion: The case of the Ligurian wedge of the northern Apennines, Italy. *Bulletin*, 123(1-2):51-70.

[46] Ogata, K. Mutti, E. Pini, Gian A. Tinterri, R. (2012). Mass transport-related stratal disruption within sedimentary mélanges: examples from the

northern Apennines (Italy) and south-central Pyrenees (Spain). *Tectonophysics*, 568:185-199.

[47] Castellarin, A. and Pini, G.A. (1989). L'arco del Sillaro: la messa in posto delle Argille Scagliose al margine appenninico padano (Appennino bolognese). *Memorie Della Società Geologica Italiana*, 39:127-142.

[48] McCall, G. and Kidd, R. (1982). The Makran, Southeastern Iran: the anatomy of a convergent plate margin active from Cretaceous to Present. Geological Society, London, Special Publications, 10(1):387-397.

[49] Sengor, A. (2003). The repeated rediscovery of mélanges and its implications for the possibility and the role of objective evidence in the scientific enterprise. SPECIAL PAPERS-GEOLOGICAL SOCIETY OF AMERICA: p. 385-446.

[50] Silver, E.A. and Beutner, E.C. (1980). Melanges. *Geology*, 8(1):32-34.

[51] Stow, D.A. and Mayall, M. (2000). Deep-water sedimentary systems: New models for the 21st century. *Marine and Petroleum Geology*, 2000. 17(2):125-135.

[52] Lucente, C.C. and Pini, G.A. (2003). Anatomy and emplacement mechanism of a large submarine slide within a Miocene foredeep in the northern Apennines, Italy: A field perspective. American Journal of Science, 303(7):565-602.

[53] Lucente, C.C. and G.A. Pini, (2008). Basin-wide mass-wasting complexes as markers of the Oligo-Miocene foredeep-accretionary wedge evolution in the northern Apennines, Italy. *Basin Research*, 20(1):49-71.

[54] Ali, S.A.; Ismail, Sabah A.; Nutman, A.P.; Bennett, V.C.; Jones, B.G.; Buckman, S.; (2016).The intra-oceanic Cretaceous (~ 108 Ma) Kata–Rash arc fragment in the Kurdistan segment of Iraqi Zagros suture zone: Implications for Neotethys evolution and closure. *Lithos*, 260:154-163.

[55] Medialdea, T. Vegas, R. Somoza, L. Vázquez, J.T. Maldonado, A. Dıaz-del-R.V. Maestro, A. Córdoba, D. Fernández-P.M (2004). Structure and evolution of the “Olistostrome” complex of the Gibraltar Arc in the Gulf of Cádiz (eastern Central Atlantic): evidence from two long seismic cross-sections. *Marine Geology*, 209(1-4):173-198.

[56] Ali, S.A. Nutman, A.P. Aswad, K.J. Jones, Brian G. (2019). Overview of the tectonic evolution of the Iraqi Zagros thrust zone: Sixty million years of Neotethyan ocean subduction. *Journal of Geodynamics*, 129:162-177.

[57] Alavi, M. (1994). Tectonics of the Zagros orogenic belt of Iran: new data and interpretations. Tectonophysics, 229(3-4):211-238.

[58] Davis, J.C. and Sampson, R.J. (1986). Statistics and data analysis in geology. *Wiley New York:* 646.

[59] Sazonov, V. (1975). Listvenitization and mineralization.*Moscow Nauka*, 30:303-313.

[60] Halls, C. and Zhao, R. (1995). Listvenite and related rocks: perspectives on terminology and mineralogy with reference to an occurrence at Cregganbaun, Co. Mayo, Republic of Ireland. *Mineralium Deposita*, 30(3):303-313.

[61] *Uịurum, A. (2000). Listwaenites in Turkey: perspectives on formation and precious metal concentration with reference to occurrences in east-central Anatolia. Ofioliti, 25(1):15-29.*

[62] Zhou, M.F. Robinson, P.T. Malpas, J. Li, Z. (1996). Podiform chromitites in the Luobusa ophiolite (southern Tibet): implications for melt-rock interaction and chromite segregation in the upper mantle. *Journal of Petrology,* 37(1):3-21.

[63] Cloos, E. and Pettijohn, F. (1973). Southern Border of the Triassic Basin, West of York, Pennsylvania: Fault or Overlap? *Geological Society of America Bulletin*, 84(2):523-536.

[64] Tucker, M.E. (1991). Sequence stratigraphy of carbonate-evaporite basins: models and application to the Upper Permian (Zechstein) of northeast England and adjoining North Sea. *Journal of the Geological Society*, 148(6):1019-1036.

[65] Galloway, W.E. and Hobday, D.K. (1996). Fuel-mineral resource base, in Terrigenous Clastic Depositional Systems, *Springer:* p. 1-5.

[66] Cronin, B.T. Çelik, H. Hurst, A. Turkmen, I. (2005). Mud prone entrenched deep-water slope channel complexes from the Eocene of eastern Turkey. *Geological Society, London, Special Publications*, 244(1):155-180.

[67] Einsele, G. (1991). Submarine mass flow deposits and turbidites. *Cycles and events in stratigraphy:* p. 313-339.

[68] Collinson, J. (1996). Alluvial sediments. Sedimentary environments: processes, facies, and stratigraphy. *Blackwell Scientific Publications*: p. 37-82.

[69] Suciu, T. Pleş, G. Tămaş, T. Bucur, I. Săsăran, E. Cociuba, I. (2021). New insights into the depositional environment and stratigraphic position of the Gugu Breccia (Pădurea Craiului Mountains, Romania). *Carnets Geol*, 21(11):215.

[70] Săsăran, E. (2006). Calcarele jurasicului superior: cretacicului inferior din Munţii Trascău. *Presa Univ:* p.5-11.

[71] Flügel, E. and Munnecke, A. (2010). Microfacies of carbonate rocks: analysis, interpretation and application. *Springer*: p. 575-586.

[72] Săsăran, E. Bucur, I. Mircescu, C.V. Ungur, C.G. (2017). Microfacies analysis and depositional environments of the Tithonian-Valanginian limestones from Dâmbovicioara Gorges (Cheile Dâmbovicioarei), Getic Carbonate Platform, Romania. *Acta Palaeontologica Romaniae*, 3(1):25-48.

[73] Mohammad, Y.O. (2011). Serpentinites and their tectonic signature along the Northwest Zagros Thrust zone, Kurdistan region, Iraq. *Arabian Journal of Geosciences*, 4(1):69-83.

[74] Aziz, N.R.; Aswad, K.J. and Koyi, H.A. (2011). Contrasting settings of serpentinite bodies in the

northwestern Zagros Suture Zone, Kurdistan Region, Iraq. *Geological Magazine*, 148(5-6):819-837.

[75] Allen, D. E. and Seyfried Jr, W. E. (2004). Serpentinization and heat generation: constraints from Lost City and Rainbow hydrothermal systems. *Geochimica et Cosmochimica Acta*, *68*(6):1347-1354

[76] Nimis, P., Zaykov, V.V.; Omenetto, P.; Melekestseva, I.Y.; Tesalina, S.G.; Orgeval, J.J.; (2008). Peculiarities of some mafic–ultramafic-and ultramafic-hosted massive sulfide deposits from the Main Uralian Fault Zone, southern Urals. *Ore Geology Reviews*, 33(1):49-69.

[77] Chi Fru, E. Kilias, S.I varsson, M. Rattray, J.E. Gkika, K. (2018). Sedimentary mechanisms of a modern banded iron formation on Milos Island, Greece. *Solid Earth*, 9(3):573-598.

[78] Dalla Torre, M.; Mählmann, R.F. and Ernst, W. (1997). Experimental study on the pressure dependence of vitrinite maturation. *Geochimica et Cosmochimica Acta*, 61(14):2921-2928.

[79] Judik, K. Rantitsch, G. Rainer, T.M. Árkai, P. Tomljenović, B. (2008). Alpine metamorphism of organic matter in metasedimentary rocks from Mt. Medvednica (Croatia). *Swiss Journal of Geosciences*, 101(3):605-616.

[80] Dunkl, I. Antolín, B. Wemmer, K. Rantitsch, G. Kienast, M. Montomoli, C. Ding, L. Carosi, R. Appel, E. El Bay, R. (2011). Metamorphic evolution of the Tethyan Himalayan flysch in SE Tibet. Geological Society, London, *Special Publications*, 353(1):45-69.

[81] Matava, T.; Matt, V. and Flannery, J. (2019). New insights on measured and calculated vitrinite reflectance. *Basin Research*, 31(2):213-227.

[82] Flores, G., 1955. Les résultats des études pour les recherches pétroliféres en Sicile:
Discussion. Proceedings of the 4th World Petroleum Congress. Casa Editrice Carlo
Colombo, Rome, pp. 121–122 (Section 1/A/2).

[83] Ayupova, N.R., Maslennikov, V.V., 2013. Biomorphic textures in the ferruginous-siliceous rocks of massive sulfide-bearing paleohydrothermal fields in the urals. Lithol. Miner. *Resour.* 48, 438–455.

تمايز الانواع الصخرية المتعددة لترسبات الأوليستوستروم المرتبطة بإثراء الحديد والتمعدن ضمن اوفيولايت منطقةجومان، شمال شرق العراق

بارزان خاناود ل عزو[1] ، كمال كولو[2] ، محمد پيروئى[2]

[1]قسم جيۆلۆجيا نەفت، كلية العلوم، جامعة سوران، سوران، العراق

[2]قسم مركز البحث العلمى (SRC) ، جامعة سوران، سوران، لعراق[2]

الملخص

تم في هذه الدراسة وصف اكتشاف رواسب الاوليستوستروم متعددة الأنواع الصخرية المرتبطة بتمعدن خام الحديد القابل للتطبيق اقتصاديًا في منطقة الرايات في شمال شرق العراق. يتم هنا خصائص تصنيف الترسيب والتمايز للانواع الصخرية المتعددة للأوليستوستروم ذات الترسيب والخصائص المتميزة من خلال البيانات البتروغرافية والمعدنية والجيوكيميائية المفصلة ، والتي سمحت بتقييم آليات التمعدن والتغيرات الحرمائية المرتبطة بها. توجد التكتلات الصخرية الحديدية أسفل الأوليستوستروم الحجر الرملي من السلسلة التي تم فحصها. لاوليستوستروم المدملكاتي الحديدي توجد طبقة من خام الحديد تحتوي على أوكسيد الحديد (حتى 14.63٪) مع كوارتز و بعض محتوى الإسبينيل الثانوي. تحت كتلة الاليستوستروم المدملكاتية الحديدية، يوج نطاق من (FOpCO) و (FSO ، الغنية أيضًا بالكوارتز والهيماتيت والكالسايت مع بعض محتوى ثانوي من الإسبنيل. المنطقة الانتقالية بسمك 2 متر (TZ) تفصل الاوليستورم الاوفيوكاربوناتي (OpCO) قليل التمعدن عن الأوليستوستروم المدملكاتي الحديدي (FCO)الأنواع الصخرية المتعددة للأوليستوستروم من أسفل إلى أعلى أوليستوستروم السربنتين (SO) ، أوليستوستروم الاوفيوكاربونيت (OPCO) ، أوليستوستروم السربنتين الحديدي (FSO) ، أولستوستروم الاوفويكاربونيت الحديدي (FOpCO)، اوليستوستروم مدملكاتي حديدي (FCO)الحديد بالإضافة الى العناصر الاقتصادية المحتملة الأخرى مثل النيكل (507 إلى 5816 مجم / كجم) ، الكوبالت (47.2 إلى 328.3 مجم / كجم). و FCO و (SstO والمنطقة الانتقالية (TZ) نشأت في قاع البحر بمزيج من التغير الحراري المائي المبكر للسربنتنايت. يعرض اكتشاف الاوليستوستروم في منطقة الرايات شمال شرق العراق كقطاع محتمل غني بالمعادن.